Available online at www.sciencedirect.com
ScienceDirect
Geochimica et Cosmochimica Acta 75 (2011) 4998–5018
Geochimica et Cosmochimica Acta
www.elsevier.com/locate/gca

Anorthosite formation by plagioclase flotation in ferrobasalt and implications for the lunar crust

Olivier Namur [a,*], Bernard Charlier [b], Cassian Pirard [c,1], Jörg Hermann [c], Jean-Paul Liégeois [d], Jacqueline Vander Auwera [a]

[a] Département de Géologie, Université de Liège, Liège, Belgium
[b] Department of Earth, Atmospheric, and Planetary Sciences, Massachusetts Institute of Technology, Cambridge, USA
[c] Research School of Earth Sciences, The Australian National University, Canberra, Australia
[d] Isotope Geology, Royal Museum for Central Africa, Tervuren, Belgium

Received 27 December 2010; accepted in revised form 10 June 2011; available online 17 June 2011

Abstract

The Sept Iles layered intrusion (Quebec, Canada) is dominated by a basal Layered Series made up of troctolites and gabbros, and by anorthosites occurring (1) at the roof of the magma chamber (100–500 m-thick) and (2) as cm- to m-size blocks in gabbros of the Layered Series. Anorthosite rocks are made up of plagioclase, with minor clinopyroxene, olivine and Fe–Ti oxide minerals. Plagioclase displays a very restricted range of compositions for major elements (An_{68}–An_{60}), trace elements (Sr: 1023–1071 ppm; Ba: 132–172 ppm) and Sr isotopic ratios ($^{87}Sr/^{86}Sr_i$: 0.70356–0.70379). This compositional range is identical to that observed in troctolites, the most primitive cumulates of the Layered Series, whereas plagioclase in layered gabbros is more evolved (An_{60}–An_{38}). The origin of Sept Iles anorthosites has been investigated by calculating the density of plagioclase and that of the evolving melts. The density of the FeO-rich tholeiitic basalt parent magma first increased from 2.70 to 2.75 g/cm^3 during early fractionation of troctolites and then decreased continuously to 2.16 g/cm^3 with fractionation of Fe–Ti oxide-bearing gabbros. Plagioclase (An_{69}–An_{60}) was initially positively buoyant and partly accumulated at the top of the magma chamber to form the roof anorthosite. With further differentiation, plagioclase ($<An_{60}$) became negatively buoyant and anorthosite stopped forming. Blocks of anorthosite (autoliths) even fell downward to the basal cumulate pile. The presence of positively buoyant plagioclase in basal troctolites is explained by the low efficiency of plagioclase flotation due to crystallization at the floor and/or minor plagioclase nucleation within the main magma body. Dense mafic minerals of the roof anorthosite are shown to have crystallized from the interstitial liquid.

The processes related to floating and sinking of plagioclase in a large and shallow layered intrusion serve as a proxy to refine the crystallization model of the lunar magma ocean and explain the vertically stratified structure of the lunar crust, with (gabbro-)noritic rocks at the base and anorthositic rocks at the top. We propose that the lunar crust mainly crystallized bottom-up. This basal crystallization formed a mafic lower crust that might have a geochemical signature similar to the magnesian-suite without KREEP contamination, while flotation of some plagioclase grains produced ferroan anorthosites in the upper crust.

1. INTRODUCTION

The role of plagioclase buoyancy and accumulation by flotation was first investigated by Bottinga and Weill (1970) and Morse (1979a) and was then recognized in the petrogenesis of plagioclase-phyric basalts that occurred in various environments, such as oceanic basalts (Flower,

* Corresponding author. Present address: Department of Earth Sciences, University of Cambridge, Cambridge, UK.
E-mail address: obn21@cam.ac.uk (O. Namur).
[1] Present address: Department of Petrology, Faculty of Earth and Life Sciences, Vrije Universiteit Amsterdam, Amsterdam, The Netherlands.

0016-7037/$ - see front matter © 2011 Elsevier Ltd. All rights reserved.
doi:10.1016/j.gca.2011.06.013

1980; Elthon, 1984; Batiza and Niu, 1992) and sub-volcanic magma chambers (Higgins and Chandrasekharam, 2007). Such plagioclase accumulation at the top of large basaltic intrusions may theoretically lead to the formation of anorthosite (Scoates, 2000). However, evidence for such process on Earth is scarce. In contrast, this apparently simple mechanism of anorthosite formation is the standard explanation for the formation of the lunar ferroan anorthosites (Wood et al., 1970; Warren, 1985, 1990). These anorthosites occur throughout the lunar upper crust (Ohtake et al., 2009), and are interpreted as the result of plagioclase flotation atop the crystallizing lunar magma ocean (LMO; Shearer et al., 2006). Earth-based remote sensing (Sprague et al., 1994), as well as color images from Mariner 10 (Robinson and Lucey, 1997) and multispectral images of MESSENGER (Blewett et al., 2009) have also tentatively identified anorthosite on Mercury, for which a magma ocean model is traditionally suggested for building of the crust (Brown and Elkins-Tanton, 2009).

The mechanism of anorthosite formation at shallow pressure contrasts with that of Proterozoic massif-type anorthosites, which requires crystallization at high pressures (Kushiro and Fuji, 1977; Emslie, 1985; Ashwal, 1993; Longhi et al., 1993, 1999; Duchesne et al., 1999). In a first stage, accumulation of buoyant plagioclase occurs at the top of deep-seated magma chambers (at 11–13 kbar), which is then followed by diapiric uprising of low-density plagioclase mushes toward mid-crustal level (3–5 kbar) due to gravitational instability. Polybaric fractional crystallization also occurs en route during the diapiric rise of the anorthosite mush (Charlier et al., 2010). Most Proterozoic anorthosites thus display evidence of continuous deformation from magmatic to solid stages. This alternative model of anorthosite formation, which is a common process on Earth, was considered as an analogue for the petrogenesis of lunar anorthosites in a post-magma ocean environment (Longhi and Ashwal, 1985; Longhi, 2003; Korotev et al., 2010). On the Moon, anorthosite diapirs are considered to be the result of plagioclase crystallization from liquids produced by remelting of overturned mafic cumulates having crystallized from the LMO (Longhi, 2003).

The Sept Iles intrusion (Canada) is the third largest layered plutonic body on Earth after the Bushveld Complex and the Dufek intrusion (see Table 1 in Namur et al., 2010). Although many layered intrusions contain anorthosite into the sequence of cumulate rocks (e.g. Bushveld: Cawthorn and Ashwal, 2009; Skaergaard: Irvine et al., 1998; Stillwater: Haskin and Salpas, 1992; Duluth: Miller and Weiblen, 1990), the Sept Iles intrusion is the only example on Earth that contains a significant volume of anorthosite exposed at the roof of the magma chamber (Higgins, 1991, 2005). Understanding the formation of anorthosite in Sept Iles may thus lead to a better comprehension of the early differentiation mechanisms of terrestrial planets and of the formation of their pristine crust.

In this study, petrographic and geochemical characteristics of the Sept Iles roof anorthosite are presented and compared to cumulate compositions crystallized at the floor. We investigate the role of magma density and its evolution with fractional crystallization in producing narrow crystallization intervals during which plagioclase was positively buoyant. Periods of plagioclase flotation alternated with plagioclase sinking, forming successively anorthosite at the top and sinking blocks of anorthosite at the base of the intrusion. These magma chamber processes characteristic of the Sept Iles intrusion are then used to propose a model that explains most of the stratigraphic features of the lunar crust and may stimulate new ideas concerning the formation and geochemical characteristics of the lunar lower crust.

2. THE SEPT ILES LAYERED INTRUSION

The Sept Iles layered intrusion is located on the north shore of the St. Lawrence River, about 500 km to the north-east of Quebec city. It is an unmetamorphosed and undeformed magmatic body, emplaced at 564 ± 4 Ma (U–Pb on zircon; Higgins and van Breemen, 1998) into high-grade gneisses of the Grenville Province. Based on the texture of some rocks in the upper part of the intrusion and on the presence of minerals indicative of low-temperature alteration in anorthositic blocks of the lower part of the intrusion, it was estimated that the Sept Iles intrusion crystallized in the pressure range between 1 and 3 kbar (Higgins, 2005).

The intrusion has a dinner-plate shape with a diameter of ca. 80 km, a maximum thickness of ca. 5.5 km and an estimated magma volume of ca. 20,000 km^3 (Loncarevic et al., 1990). The north-western part of the intrusion crops out around the Sept Iles peninsula and on islands of the Sept Iles archipelago, where three different series have been described: the Layered Series, the Upper Border Series and the Upper Series (Fig. 1; Higgins, 2005).

The ca. 4.7 km-thick Layered Series is made up of 3 megacyclic units (MCU) showing the following succession of cumulus assemblages: troctolite (plagioclase and olivine), Fe–Ti oxide-bearing troctolite (plagioclase, olivine, Fe–Ti oxide minerals) and layered gabbro (plagioclase, Fe–Ti oxide minerals, clinopyroxene, ± olivine, ± apatite; Namur et al., 2010). Cumulus olivine is locally absent from the gabbro sequence (olivine hiatus; Morse, 1990). Each unit results from the crystallization of a new influx of ferrobasaltic parent magma (Namur et al., 2010). Six small magma chamber replenishments also occurred during the crystallization of MCU II (Fig. 1b). The Sept Iles Layered Series is characterized by the presence of abundant cm- to m-scale anorthositic blocks (autoliths) included in gabbroic rocks (Higgins, 2005).

The Upper Border Series is made up of anorthosite, with minor leucotroctolite and leucogabbro (Higgins, 1991). It also contains many cm- to dm-scale pods of granophyre, mainly syenitic to granitic in composition. The total thickness of this series is not perfectly known but is estimated to be in the range from 100 to 500 m.

The Upper Series is made up of ferroan metaluminous syenite and granite with minor monzonite (Higgins and Doig, 1986; Namur et al., 2011). It is found as small cupolas topping the central part of the intrusion. Namur et al.

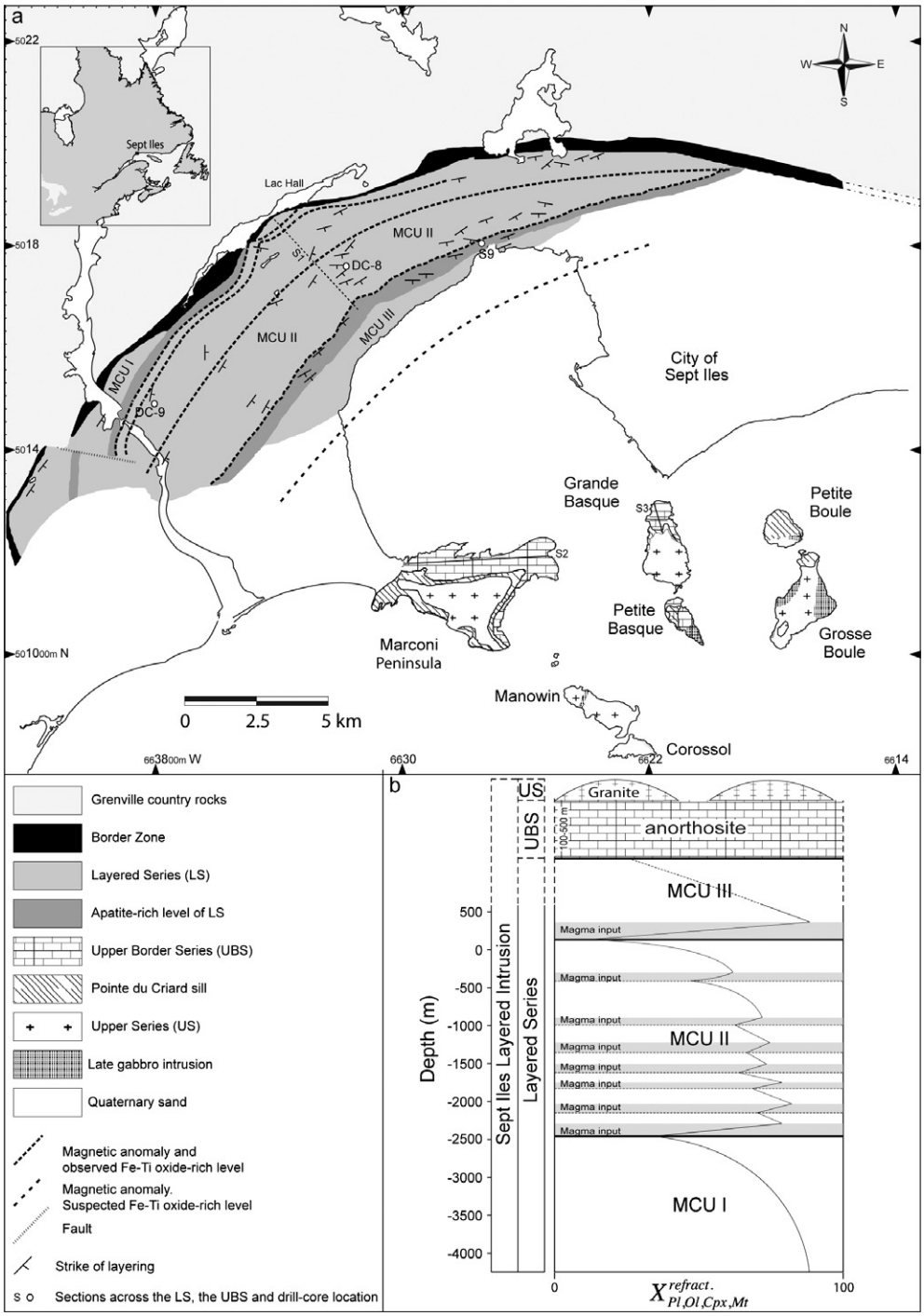

Fig. 1. (a) Geological map of the Sept Iles layered intrusion adapted from Higgins (2005). Inset map in the upper-left-corner shows the location of the map area in the south-eastern part of Canada. (b) Schematic stratigraphic column of the Sept Iles layered intrusion with evolution of mineral compositions (Xrefract: An-content of plagioclase, Fo-content of olivine, Mg# of clinopyroxene and Cr-content of magnetite) in the Layered Series. Horizontal dashed lines in MCU II represent the end of successive small differentiation cycles. Horizontal grey bands in MCU II and at the bottom of MCU III represent stratigraphic intervals with reverse evolution of mineral compositions as a result of magma chamber replenishments. The "0-meter" reference level corresponds to the first appearance of cumulus apatite in MCU II. MCU = megacyclic unit.

(2011) showed that rocks from the Upper Series represent evolved residual liquids left after extensive fractionation of the Layered Series and the Upper Border Series from the Sept Iles ferrobasaltic parent magma.

3. SAMPLING

Ten anorthositic samples were collected in the Upper Border Series. Eight samples (prefix M) come from a

W–E section along the north coast of the Marconi Peninsula (S2 in Fig. 1a) and two samples (prefix GB) come from the northern part of the Grande Basque Island (S3 in Fig. 1a). Fifty-three other anorthositic samples were collected in autoliths from the Layered Series. Most of them come from three drill-cores (DC-9, 36 samples; DC-8, 12 samples; s9, 2 samples; Fig. 1a). Three surface samples were also collected along the N–S Lac Hall section (S1 in Fig. 1a) through the MCU II of the Layered Series. Forty-one troctolite-gabbro cumulate samples from the Layered Series MCU I, previously presented in Namur et al. (2010), were also selected for new Sr-isotope analyses, trace element analyses of olivine and Ca-rich pyroxene and electron microprobe analyses of plagioclase cores. For autolith and cumulate samples, stratigraphic positions are reported in meters with the "0 meter" reference level corresponding to the appearance of cumulus apatite in MCU II. Analytical methods, including all the preparation techniques and instrument protocols, are described in Electronic Annex.

4. FIELD RELATIONSHIPS AND PETROGRAPHY

4.1. Anorthosite rocks of the Upper Border Series

Mineral proportions indicate that the term anorthosite s.s. (>90 vol.% of plagioclase) cannot be strictly used to define part of the samples from the Upper Border Series (Fig. 2; Table EA1; Electronic Annex). This name will nevertheless be used collectively in the following to describe plagioclase-rich rocks, properly referred to as leucogabbro, leucotroctolite and anorthosite. The Upper Border Series comprises both massive and laminated anorthosites (Fig. 3; Higgins, 1991). Massive anorthosite constitutes over 90 vol.% of the Upper Border Series. Both types of anorthosite locally contain interstitial syenitic to granitic material (Fig. 3) that results from the percolation of highly evolved liquids through the not fully-solidified anorthositic rocks of the Upper Border Series (Namur et al., 2011).

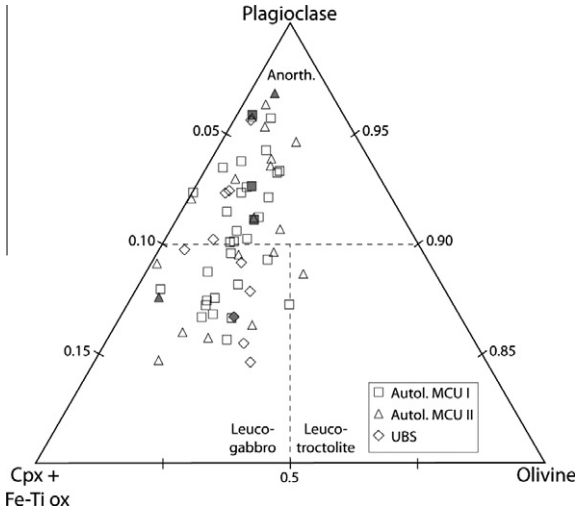

Fig. 2. Mineral proportions (vol.%) in Sept Iles anorthosite samples from the Upper Border Series and in autoliths from the Layered Series. Ternary diagram showing the relative amounts of plagioclase and mafic minerals (Fe–Ti oxide minerals + clinopyroxene and olivine). Anorth = anorthosite; Autol = autolith. Open symbols: massive anorthosite samples, filled symbols: laminated anorthosite samples.

Massive anorthosites are comprised of randomly oriented subhedral to euhedral plagioclase (Fig. 4a), with minor olivine, clinopyroxene, Fe–Ti oxide minerals (ilmenite–hematite and magnetite-ulvöspinel solid solutions), apatite, quartz, K-feldspar, amphibole, sulfides and minerals resulting from low-temperature hydrothermal alteration (calcite, chlorite, serpentine and epidote). Plagioclase (modal proportion: 84–95 vol.%; Fig. 2; Table EA1) forms distinctively zoned sub-equant to strongly tabular grains, ranging in size from 0.1 to 40 mm (Fig. 4a). Olivine (1–6 vol.%) occurs as: (1) disseminated mm-scale optically unzoned anhedral to subhedral grains of sub-equant to slightly elongated shape and (2) mm- to cm-scale unzoned poikilitic grains enclosing lath-shaped plagioclase grains (Fig. 4b). Clinopyroxene (3–8 vol.%) is represented by mm- to cm-scale unzoned poikilitic grains (Fig. 4a and c) containing abundant oriented exsolution lamellae of Fe–Ti oxide minerals and orthopyroxene, and Schiller inclusions. Fe–Ti oxide minerals (0–3 vol.%) form polycrystalline aggregates with anhedral texture and size up to 5 mm in diameter. Laminated anorthosites show mineralogical characteristics similar to those of the massive rocks, except that plagioclase grains display a very well defined igneous lamination (Fig. 4d and e).

4.2. Anorthosite autoliths in the Layered Series

Abundant cm- to tens of m-large anorthositic blocks (autoliths; Fig. 3d) occur in the Layered Series. They are mostly slab-like in shape but some of them are isometric. Their contacts with cumulate rocks of the Layered Series are angular to slightly-rounded and the layering is deformed beneath them and smoothed above. Two types of autolith blocks occur in the Layered Series: the first one, which is by far the most abundant, is made up of massive anorthosite, while the second one comprises laminated anorthosite.

Massive and laminated autoliths have mineralogical assemblages and mineral textures similar to those of anorthositic rocks from the Upper Border Series (Fig. 4f). Their stratigraphic distribution in the Layered Series was determined through examination of rocks intersected by the drill-cores (DC-9; DC-8; s9) and exposed along two field N–S cross-sections. Seventy-two autolith blocks were numbered and occur abundantly from the middle part of MCU I to the lower part of MCU III (Fig. 5; Table EA2; Electronic Annex). This 4100 m-thick stratigraphic interval is mostly made up of gabbro and minor Fe–Ti oxide-bearing troctolite. No autoliths were observed in troctolites from the lower part of MCU I and the upper part of MCU III (Fig. 5). Due to continuous outcrops in these stratigraphic intervals, this absence is interpreted as a genuine feature of petrological significance.

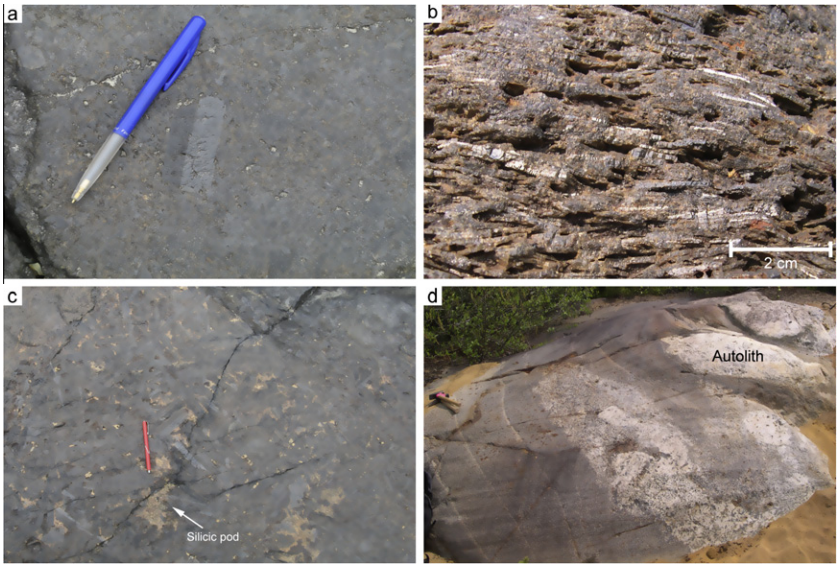

Fig. 3. Photographs of macroscopic structures of anorthosites in the Sept Iles Layered Series and Upper Border Series. (a) Massive anorthosite of the Upper Border Series displaying a 5 cm-long plagioclase crystal comprised in a matrix of smaller plagioclase grains. (b) Laminated anorthosite from the Upper Border Series. Altered clinopyroxene oikocrysts have been weathered out. (c) Massive anorthosite from the Upper Border Series showing interstitial syenitic to granitic material between plagioclase crystals. (d) Meter-scale anorthosite block (autolith) in gabbro from the Layered Series MCU II.

5. RESULTS

5.1. Mineral composition in cumulates from the Layered Series

In cumulate rocks from the Layered Series, the An-content of plagioclase decreases upwards in each MCU, from the most primitive troctolites (An_{69}–An_{62}) to Fe–Ti oxide-bearing troctolites (An_{62}–An_{60}) and the most evolved gabbros (An_{60}–An_{34}; Fig. 5; Tables EA3 and EA4; Electronic Annex). Strontium and Ba in plagioclase increase continuously from troctolites (Sr: 1030–1070 ppm; Ba: 120–140 ppm) to Fe–Ti oxide-bearing troctolites (Sr: 1040–1090 ppm; Ba: 140–170 ppm) and gabbros (Sr: 1040–1620 ppm; Ba: 150–680 ppm; Figs. 5 and 6a, b; Tables EA3 and EA4). The REE patterns of plagioclase-cores are characterized by LREE-enrichment and by a positive Eu anomaly (Table EA4). In most samples, HREE are below detection limit. The positive Eu anomaly continuously increases from the troctolites (Eu/Eu^*: 9.1–15.3) to Fe–Ti oxide-bearing troctolites (14.8–17.0) and gabbros (18.9–46.5; Fig. 6c).

The refractory components of olivine and clinopyroxene (olivine forsterite-content and clinopyroxene Mg#; molar MgO/(FeO + MgO)) also decrease continuously upwards in each MCU from troctolites (Fo: 73–67; cpx-Mg#: 79–74) to Fe–Ti oxide-bearing troctolites (Fo: 67–65; cpx-Mg#: 76–73) and gabbros (Fo: 66–55; cpx-Mg#: 75–69; Figs. 1b and 7a, b). Compatible trace element-contents of mafic minerals (Ni, Co and Cr in olivine and clinopyroxene) also decrease continuously from troctolites to gabbros (e.g. Ni in olivine in Fig 7c and Cr in clinopyroxene in Fig. 7d; Table EA5; Electronic Annex). Interstitial clinopyroxene in troctolites and Fe–Ti oxide-bearing troctolites has high REE-contents (e.g. La: 6–21 times La of CI-chondrite; Fig. 8a; Table EA5) and show REE-patterns with significant negative Eu anomalies (Eu/Eu^*: 0.51–0.93). In contrast, cumulus clinopyroxene from gabbros has lower REE-contents (e.g. La: 6–12 times La of CI-chondrite; Fig. 8b) and shows REE-patterns with neutral to slightly positive Eu anomalies (Eu/Eu^*: 1.0–1.5).

5.2. Mineral compositions in anorthosites

Plagioclase-cores of the anorthosite samples from the Upper Border Series and autoliths of the Layered Series show a relatively restricted range of compositions (An_{68}–An_{60}; Sr: 1023–1071 ppm; Ba: 123–172 ppm; Figs. 5 and 6; Table EA6; Electronic Annex). Data from electron microprobe profiles through plagioclase grains and detailed analyses of rims indicate that plagioclase grains from anorthosites are strongly compositionally zoned. They show a central plateau with cumulus core-compositions in the range between An_{68} and An_{60}, rimmed by compositions evolving down to ca. An_{50}, while most rims cluster around $An_{60\pm3}$ (Figs. 9 and 10). The REE patterns of plagioclase-cores are characterized by LREE-enrichment, and by a positive Eu anomaly (Eu/Eu^*: 9.6–16.8; Fig. 6c).

Olivine and clinopyroxene also show narrow ranges of major element compositions (olivine: $Fo_{66–61}$; Fig. 7a; Table EA7; Electronic Annex and clinopyroxene: cpx-$Mg\#_{75–67}$; Fig. 7b; Table EA8; Electronic Annex). In contrast, compatible trace elements display larger compositional ranges (olivine: Ni: 189–846 ppm, Co: 192–247 ppm; clinopyroxene: Ni: 10.4–163 ppm, Co: 35.7–48.2 ppm, Cr: 1.21–194 ppm; Fig. 7c and d). Clinopyroxene-grains from all the anorthositic samples are characterized by high-REE contents (e.g. La: 10–58 times La in CI-chondrite; Fig. 8c) and negative Eu anomalies (Eu/Eu^*: 0.35–0.95).

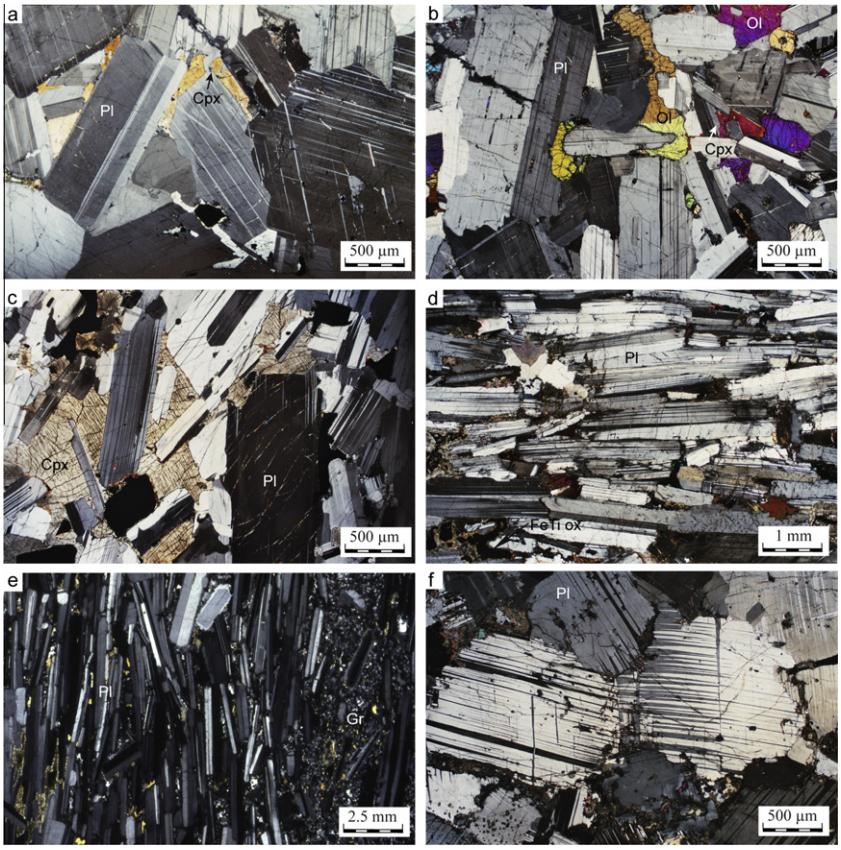

Fig. 4. Photomicrographs of mineral assemblages and textures in anorthosite rocks of the Upper Border Series and in autolith blocks of the Layered Series. (a) Massive anorthosite from the Upper Border Series showing zoned mm-scale plagioclase grains and interstitial poikilitic clinopyroxene. Sample GB-05–04, cross-polarized transmitted light. (b) Massive anorthosite from the Upper Border Series showing tablet-shaped mm-scale plagioclase grains and interstitial poikilitic olivine and clinopyroxene. Sample M-07–55, cross-polarized transmitted light. (c) Massive anorthosite with mm-scale interstitial poikilitic clinopyroxene. Sample M-07–17, cross-polarized transmitted light. (d) Strongly laminated anorthosite from the Upper Border Series with large plagioclase grains, minor Fe–Ti oxide minerals and biotite in replacement of primary ferromagnesian minerals. Sample GB-X1, cross-polarized transmitted light. (e) Strongly laminated anorthosite from the Upper Border Series with fine-grained interstitial granitic material dominated by quartz, K-feldspar and amphibole. Cross-polarized transmitted light. Picture from M.D. Higgins. (f) Massive anorthosite autolith from the Layered Series with large plagioclase grains and minor hydrothermal alteration phases. Curved plagioclase twinning results from mineral deformation probably due to the weight of overlying cumulate rocks. Sample DC-9–762.5, autolith-44, MCU I, cross-polarized transmitted light. Pl: plagioclase, FeTi ox: Fe–Ti oxide minerals; Gr: granitic material.

5.3. Bulk anorthosite compositions

Whole-rock compositions are used to determine mineral proportions in anorthosite samples (see Electronic Annex) and will be used in the following to determine the proportion of trapped liquid having crystallized in these samples. Anorthosite rocks of the Upper Border Series and autoliths of the Layered Series have similar whole-rock compositions in terms of major and trace elements (Table EA9; Electronic Annex). Their high contents in SiO_2 (45.8–52.8 wt.%), Al_2O_3 (23.1–29.1 wt.%), CaO (9.6–13.1 wt.%), Na_2O (2.5–4.5 wt.%) and Sr (701–923 ppm) reflect the plagioclase-rich nature of these rocks. The variation of the FeO_t (0.7–7.2 wt.%), TiO_2 (0.1–2.6 wt.%), MgO (0.2–4.8 wt.%) and P_2O_5 (0.05–0.25 wt.%) contents mirror the variable amount of mafic minerals (olivine, Ca-rich pyroxene and Fe–Ti oxides) and apatite.

5.4. Strontium isotopes

Sr-isotope ratios ($^{87}Sr/^{86}Sr$) were measured on plagioclase (± quartz) separates from anorthosites of the Upper Border Series, from autoliths of the Layered Series and from cumulate rocks of the Layered Series (Table EA10; Electronic Annex). Isotope ratios were re-calculated for an age of 564 Ma (Higgins and van Breemen, 1998). In cumulate rocks of the Layered Series, Sr-isotope ratios increase upwards in each MCU from the most primitive troctolites (0.7036–0.7039) to the Fe–Ti oxide-bearing troctolites (0.7038–0.7040) and the most evolved gabbros (0.7040–0.7049; Figs. 5 and 6d; Tables EA3 and EA10) because of a slight contamination by highly radiogenic gneissic country rocks (Namur et al., 2011). Anorthosite samples show restricted ranges of isotopic ratios, from 0.70356 to 0.70379 for the Upper Border Series, and from 0.70369 to

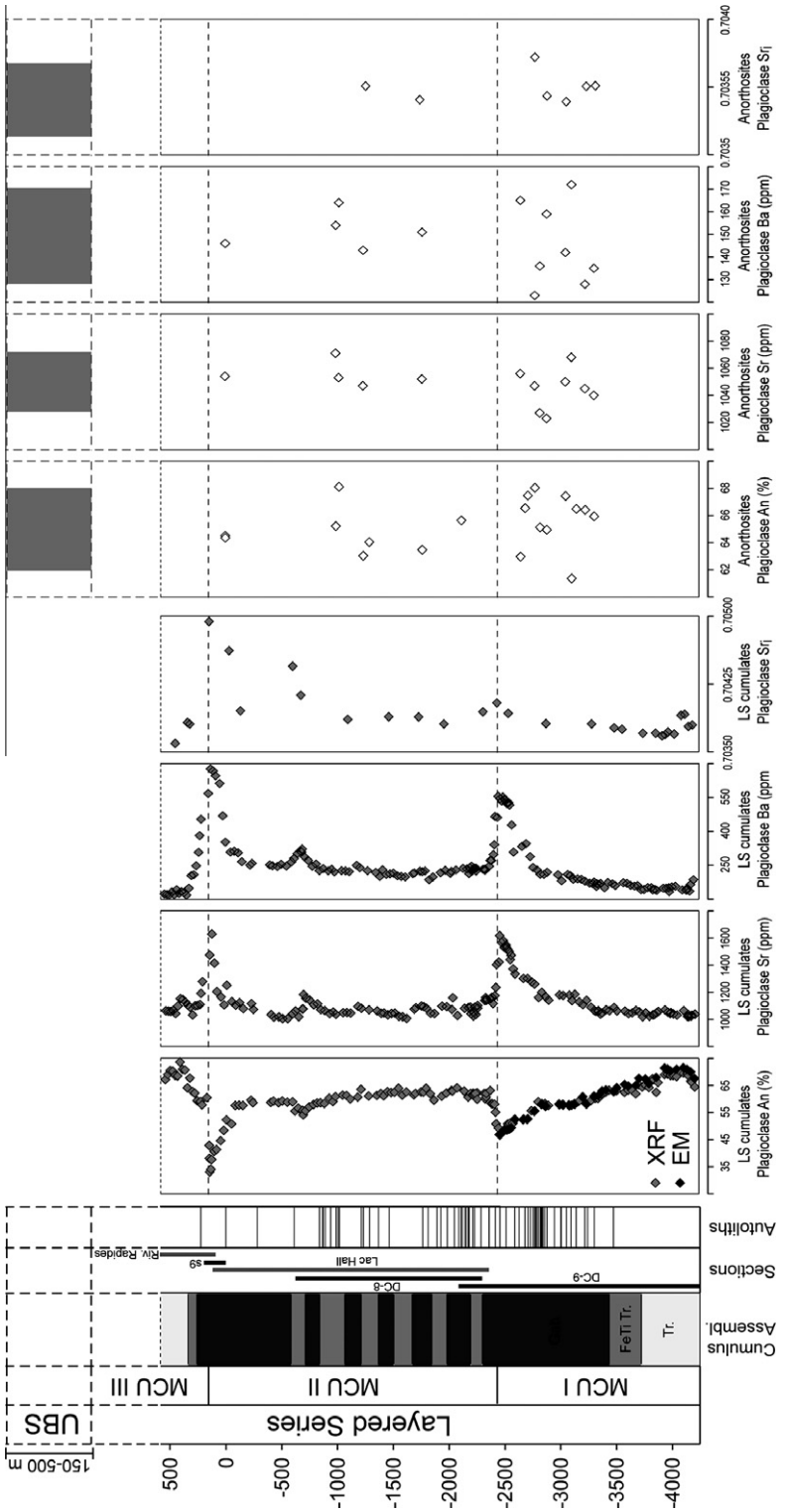

Fig. 5. Stratigraphic column of the Sept Iles intrusion showing the distribution of rock-types (troctolite; Fe–Ti oxide bearing troctolite; gabbro) in the Layered Series, the stratigraphic intervals intersected by the sections and drill-cores investigated in this study and the distribution of autolith blocks in the Layered Series. Compositions of plagioclase (An%, Sr, Ba, $^{87}Sr/^{86}Sr$) are also presented for cumulate rocks of the Layered Series, for anorthosites of the Upper Border Series and for autolith blocks of the Layered Series. Note the different scales for cumulate samples and for anorthosite samples. The range of plagioclase compositions in the Upper Border Series are represented by a grey field as no stratigraphic position can be precisely determined for the samples. Tr = troctolite; FeTi Tr = Fe–Ti oxide-bearing troctolite; Gab = gabbro; XRF = X-ray fluorescence analyses; EM = electron microprobe analyses.

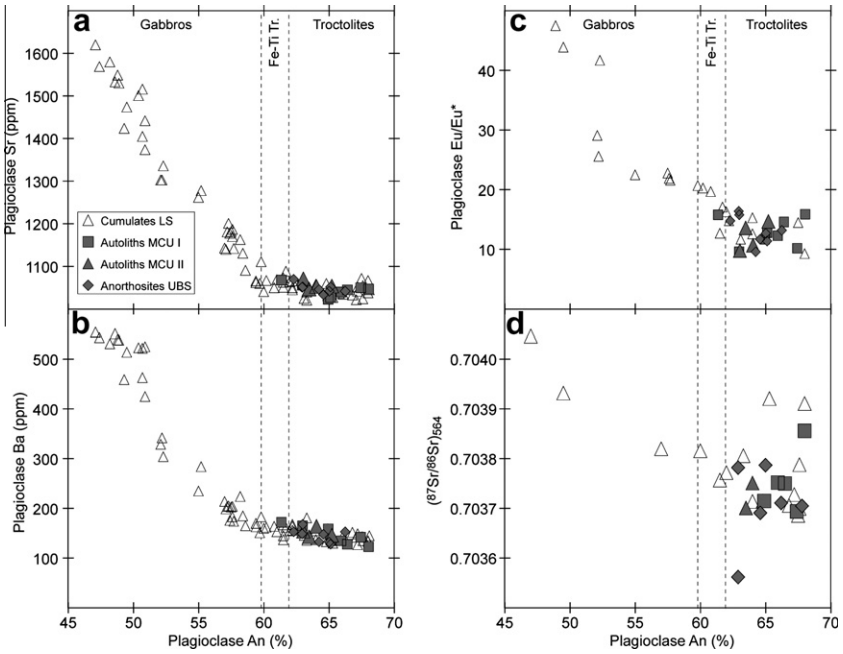

Fig. 6. Major and trace element compositions, and Sr-isotope ratios of plagioclase from cumulates of the Layered Series and anorthosites of the Upper Border Series and in autoliths of the Layered Series. (a) Sr (ppm) vs. An (%). (b) Ba (ppm) vs. An (%). (c) Eu anomaly (Eu/Eu^*) vs. An (%). (d) $(^{87}Sr/^{86}Sr)_{564}$ vs. An (%).

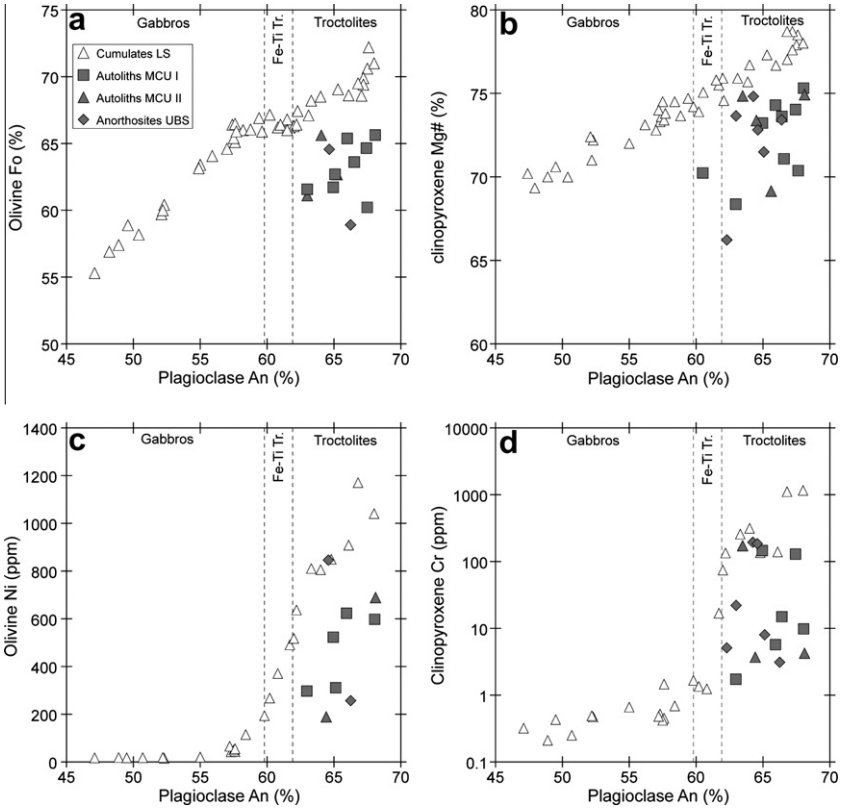

Fig. 7. Comparison between mineral compositions in anorthosites and in cumulate rocks of the Layered Series. (a) Olivine Fo (%) vs. plagioclase An (%). (b) Clinopyroxene Mg# (%) vs. plagioclase An (%). (c) Olivine Ni (ppm) vs. plagioclase An (%). (d) Clinopyroxene Cr (ppm) vs. plagioclase An (%). Olivine Fo and Clinopyroxene Mg# data for the Layered Series are from Namur et al. (2010).

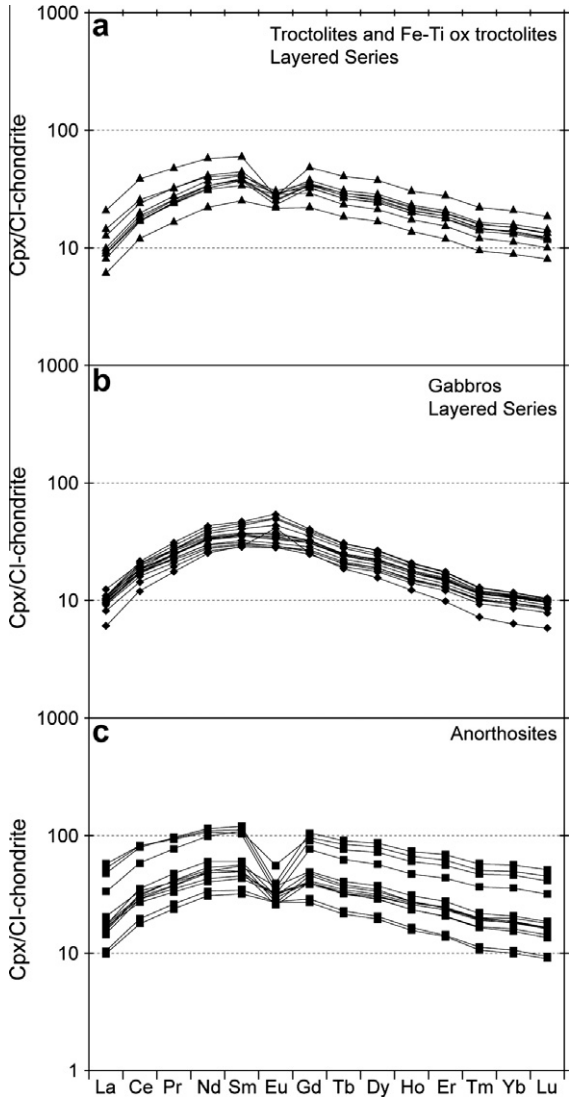

Fig. 8. REE patterns of clinopyroxene. (a) Clinopyroxenes from troctolites and Fe–Ti oxide-bearing troctolites units of the Layered Series. (b) Clinopyroxenes from gabbros of the Layered Series. (c) Clinopyroxenes from anorthosites of the Layered Series and the Upper Border Series. CI-chondrite composition from Sun and McDonough (1989).

0.70386 for autoliths (Figs. 5 and 6; Table EA10). When plotted against the stratigraphic height in the Layered Series, no evolutional trend is observed for Sr-isotope compositions of autoliths (Fig. 5).

6. DISCUSSION

6.1. Comparing plagioclase compositions in anorthosites and basal cumulates

Plagioclases in anorthosites of the Upper Border Series and in autoliths of the Layered Series show a similar range of compositions for both major (An-content; Figs. 5 and 6) and trace (Sr, Ba and Eu/Eu*; Fig. 6a–c) elements. All the anorthosite samples have also similar Sr-isotope ratios (Fig. 6d). This obvious similarity in plagioclase composition suggests that the Upper Border Series and autoliths of the Layered Series are genetically linked.

Compared to cumulate rocks of the Layered Series, plagioclase from anorthosites shows a very restricted range of major-, trace- and isotopic-compositions, which is highly similar to that observed in troctolites and Fe–Ti oxide-bearing troctolites (Figs. 5 and 6). In contrast, gabbros from the Layered Series show more evolved (lower An-content, higher Sr- and Ba-contents; Fig. 6a and b) and more radiogenic (Fig. 6d) plagioclase compositions. The similarity between major and trace element compositions as well as Sr-isotope ratios between plagioclase in anorthosites and in basal troctolites and Fe–Ti oxide-bearing troctolites of the Layered Series suggest that plagioclase from all these rocks has crystallized at the same time from the same parent magma.

6.2. Formation of Sept Iles anorthosites

6.2.1. Sept Iles liquid line of descent and density calculations

The Sept Iles parent magma is inferred to be a tholeiitic basalt (ferrobasalt; 48 wt.% SiO_2; 15 wt.% FeO_t; Namur et al., 2010), slightly richer in FeO_t than that of the Skaergaard intrusion (12–13 wt.% FeO_t; Hoover, 1989; Toplis and Carroll, 1995, 1996; Nielsen, 2004; Jakobsen et al., 2010) and similar to that of the Bjerkreim-Sokndal intrusion (Vander Auwera and Longhi, 1994). The Sept Iles liquid line of descent (LLD) has the following characteristics (Namur et al., 2011): (1) crystallization of troctolites drives the parent magma on a tholeiitic trend with FeO_t-enrichment (up to 17 wt.%) and slight SiO_2-depletion (down to 47 wt.%); (2) saturation of Fe–Ti oxide minerals and clinopyroxene drives the residual liquid along a FeO_t-depletion and SiO_2-enrichment trend, ultimately leading to the formation of A-type granites (67–76 wt.% SiO_2) at the top of the magma chamber. The precise knowledge of the LLD allows calculation of the evolution of melt density with differentiation.

Density calculations were performed following the expression of Bottinga and Weill (1970), with partial molar volume, thermal expansion and compressibility data of Lange and Carmichael (1987), Kress and Carmichael (1991), Toplis et al. (1994), Lange (1997), Ochs and Lange (1997, 1999). Calculations of liquid densities require knowledge of the following intensive variables: (1) the evolution of oxygen fugacity (fO_2) with differentiation; (2) the H_2O-content of the melt; (3) the melt liquidus temperatures and (4) the pressure of crystallization.

The fO_2 of the Sept Iles intrusion has not yet been estimated. However, as the Sept Iles and Skaergaard intrusions have similar parental magmas and cumulus mineral assemblages (McBirney, 1996; Namur et al., 2010), results obtained for the Skaergaard are used here. The oxygen fugacity in the Skaergaard intrusion has been constrained to be close to the FMQ buffer during the crystallization Fe–Ti oxide-free cumulates and to decrease to FMQ-1 after the saturation of magnetite (Osborn, 1959; Forst and Lindsley, 1992; Thy et al., 2009). In this study, density calculations were realized at FMQ for liquids not saturated in

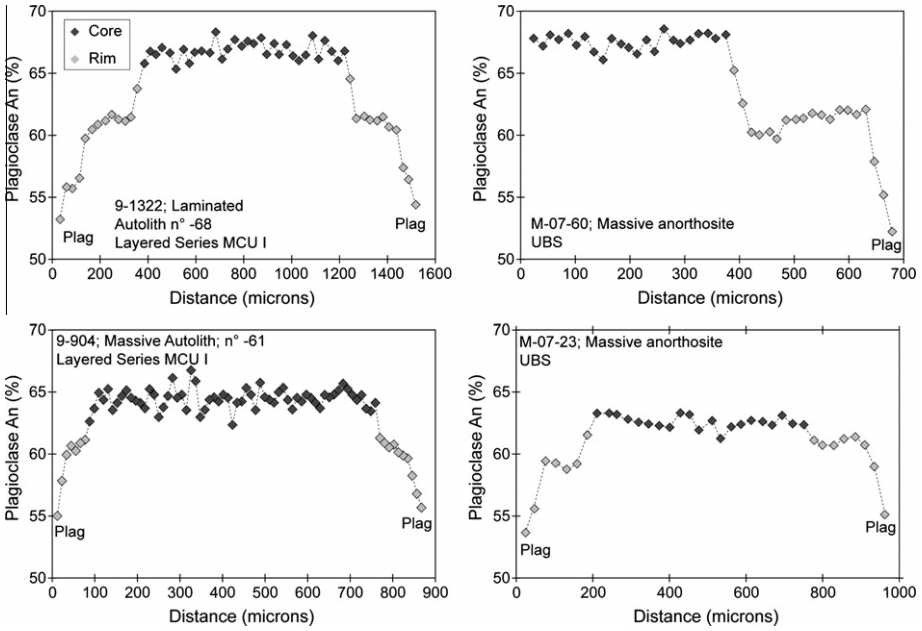

Fig. 9. Selection of compositional profiles (plagioclase An%) across representative plagioclase grains from samples of anorthosite from the Layered Series and the Upper Border Series. The nature of the phase in contact with the plagioclase is indicated. The distance scale is taken from an arbitrary starting point and only relative distances bear some significance.

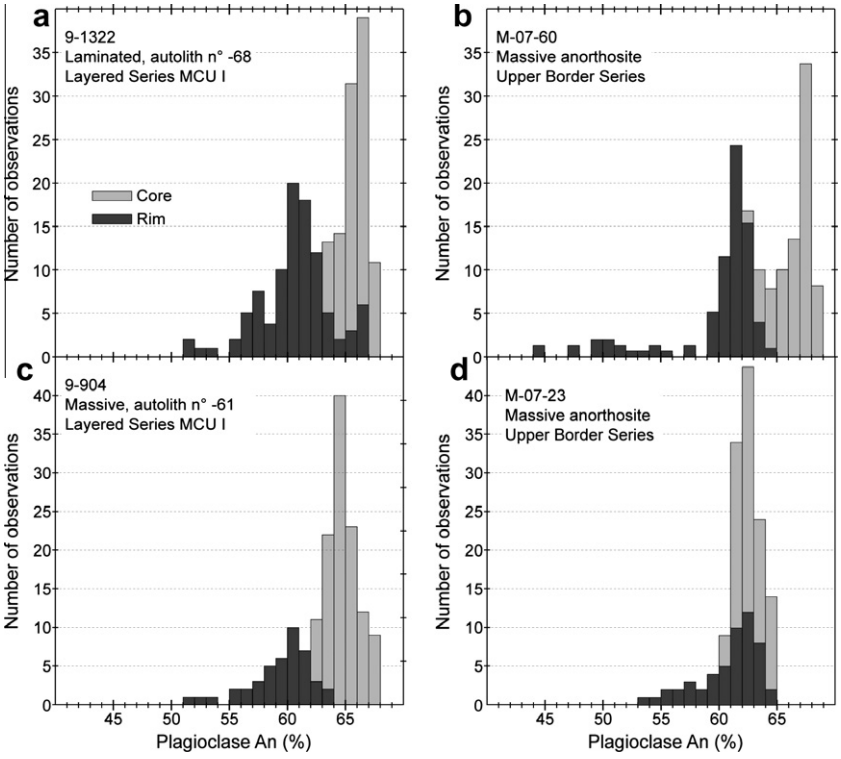

Fig. 10. Histograms of plagioclase compositions (An%) for 4 samples of anorthosite from the Layered Series and the Upper Border Series. Note that the data for the different An-contents are stacked and not overlapped.

Fe–Ti oxide minerals. For Fe–Ti oxide saturated liquids, we used values varying linearly with the silica-content from FMQ (at 47 wt.% SiO_2) to FMQ-1 (at 60 wt.% SiO_2).

Sept Iles granites contain H_2O- (0.8–1.5 wt.%) and F- (0.7–2.4 wt.%) rich brown hornblende (Namur et al., 2011). The occurrence of this mineral allows us to constrain

the H_2O-content of granitic liquids to be at least 4 wt.% (Dall'Agnol et al., 1999; Klimm et al., 2003; Bogaerts et al., 2006). Using geochemical modeling for major and trace elements, Namur et al. (2011) have shown that the Sept Iles granitic melts are reached after 90% of fractionation. This enables us to estimate the H_2O-content of the parent magma at ca. 0.4 wt.%. Density calculations were performed with liquid H_2O-contents increasing from 0.4 wt.% H_2O in the parent magma to 4 wt.% H_2O in the most evolved granitic compositions.

Liquidus temperatures were calculated using the linear relationship between liquidus temperature and the MgO-content of ferrobasaltic melts observed in experiments of Toplis and Carroll (1995). The liquidus temperature of the Sept Iles parent magma was calculated to be ca. 1155 °C, while Fe–Ti oxide minerals and apatite saturated at 1120 °C and 1090 °C, respectively. The pressure of intrusion is estimated to be 1–3 kbar (Higgins, 2005).

The compositions of plagioclase (An%) crystallizing in equilibrium with Sept Iles liquids along the LLD were calculated using empirical equations for plagioclase-melt equilibria from Namur et al. (in press). Calculated plagioclase compositions were corrected for the effects of the melt H_2O-content (0.4–4 wt.%) and the pressure (1 kbar) using the equations of Putirka (2005). Plagioclase densities were calculated at the liquidus temperatures by considering a linear relationship between the densities of albite (2.62 g/cm^3 at 298 K; Campbell et al., 1978) and anorthite (2.76 g/cm^3 at 298 K) and using the thermal expansion coefficients of Niu and Batiza (1991).

6.2.2. Relation between magma and plagioclase densities

The calculated density of the Sept Iles parent magma, using the constraints explained in the last section, is 2.70 g/cm^3 at 1155 °C. During fractionation of troctolites, the melt density increased to 2.75 g/cm^3 at ca. 1120 °C, before decreasing continuously to 2.16 g/cm^3 for granitic melts at ca. 995 °C, as a result of fractionation of Fe–Ti oxide-bearing troctolites and gabbros (Fig. 11a; Table EA11; Electronic Annex). This trend is similar to that observed for typical tholeiitic liquid lines of descent (Campbell et al., 1978; Sparks et al., 1980; Sparks and Huppert, 1984; Morse, 1986, 1988; Hunter and Sparks, 1987).

Calculated compositions of plagioclase crystallizing along the Sept Iles LLD range from An_{68} to An_{34}, in excellent agreement with plagioclase compositions observed in the Layered Series (Namur et al., 2010). Plagioclase densities evolved with differentiation from 2.69 to 2.64 g/cm^3 (Fig. 11a).

Results of density calculations indicate that plagioclase was positively buoyant in primitive melts. However, plagioclase became denser than the residual melt soon after saturation of Fe–Ti oxide minerals, when the melt reached 49 wt.% SiO_2 (fraction of residual liquid; $F = 72\%$; Namur et al., 2011; Fig. 11a and b). Primitive liquids with less than 49 wt.% SiO_2 are in equilibrium with a narrow range of plagioclase compositions (An_{69}–An_{60}; Fig. 11c), which were thus positively buoyant. Liquids containing more than 49 wt.% SiO_2 are less dense than the plagioclases in

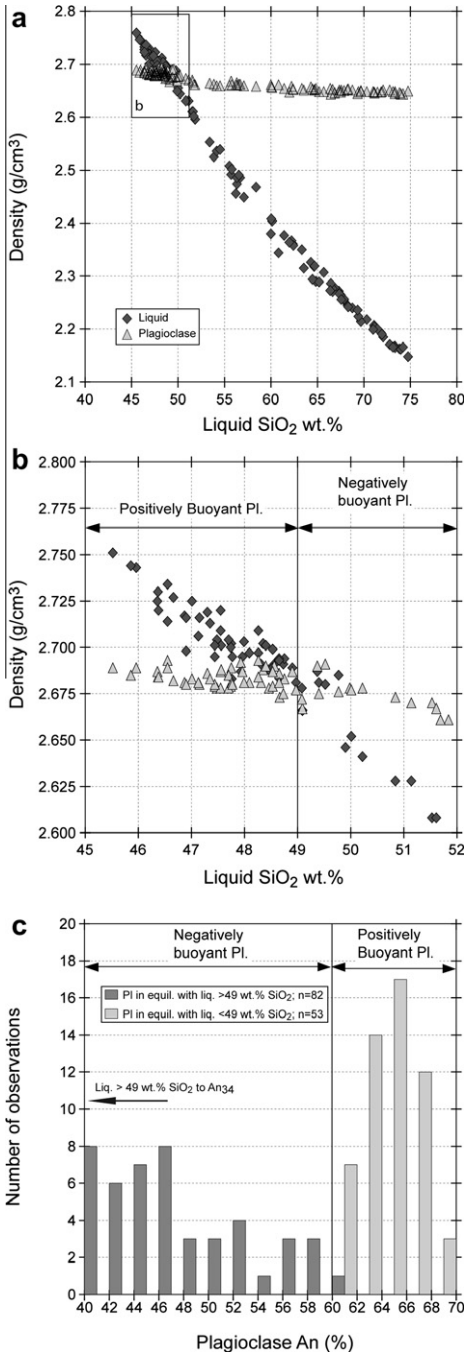

Fig. 11. (a) Density evolution of Sept Iles liquids and equilibrium plagioclases with differentiation (wt.% SiO_2 in the liquid). Density calculations are based on liquid compositions presented by Namur et al. (2011) and plagioclase compositions calculated using equations of Namur et al. (in press). See text for the methodology of density calculations. The rectangle in the upper-left part of the diagram shows the field view of Fig. 4b. (b) Close up on the plagioclase and liquid density curves crossing. Plagioclase is buoyant on liquids with less than 49 wt.% SiO_2, while it is non-buoyant on more evolved liquids. (c) Histogram showing calculated compositions (An%) of buoyant plagioclase in equilibrium with liquids having less than 49 wt.% SiO_2 and non-buoyant plagioclase in equilibrium with evolved liquids (more than 49 wt.% SiO_2).

equilibrium with them ($An_{\leqslant 60}$; Fig. 11b and c) and plagioclase flotation was therefore no longer a potentially operative mechanism. After Fe–Ti oxide mineral saturation, primitive plagioclase grains (An_{69}–An_{60}) accumulated at the roof of the intrusion, thus became denser than the main magma body and may have sunk into the magma, explaining the presence of anorthosite autolith blocks in gabbros of the Layered Series.

6.2.3. *Mechanisms of plagioclase flotation*

Plagioclase An_{69}–An_{60} is buoyant on Sept Iles basaltic melts, in excellent agreement with the occurrence of this range of compositions in anorthositic rocks of the Upper Border Series and in the autoliths found in the Layered Series (Fig. 12). However, as previously illustrated, plagioclases with similar major and trace element compositions than those of the anorthosites are also abundantly observed in the floor cumulates of the Layered Series (troctolites and Fe–Ti oxide-bearing troctolites; Figs. 6 and 12). This means that not all plagioclase grains with composition more primitive than An_{60} have accumulated at the roof of the magma chamber. In the following, the efficiency of plagioclase flotation is quantified and discussed in light of published theoretical and experimental crystallization models for mafic magma chambers.

Cooling of basaltic magma chambers dominantly occurs at the roof (e.g. Irvine, 1970; Brandeis and Jaupart, 1986; Morse, 1986; Martin et al., 1987; Kerr et al., 1990). However, in large aspect-ratio magma chambers, such as Sept Iles, Bushveld and Stillwater, crystallization essentially occurs at the bottom of the magma chamber (Campbell, 1978, 1996; Huppert and Sparks, 1980; Brandeis et al., 1984; Brandeis and Jaupart, 1986; Martin et al., 1987; Martin, 1990; Latypov, 2003). This results from convective instabilities at the top of the chamber that hamper the attachment of the crystals against the roof (Brandeis and Jaupart, 1986), from the effect of pressure on the liquidus temperature that facilitates nucleation at the floor of the magma chamber (Irvine, 1970; Martin, 1990) and from the low degree of supercooling that is required for the nucleation process (Brandeis et al., 1984; Campbell, 1996). Nucleation at the roof and transportation of the crystals to the floor by convection currents is also generally envisaged as a crystallization model for basaltic magma chambers (e.g. Morse, 1986, 1988; Philpotts and Dickson, 2000). However, when occurring, part of the crystals stay attached at the roof and form a "downward roof cumulate sequence", as exemplified in the Skaergaard or Kiglapait intrusions (Morse, 1979b; McBirney, 1996). Moreover, in these intrusions the floor cumulate sequence is significantly thicker than the roof sequence, suggesting that floor nucleation may have also occurred (Brandeis and Jaupart, 1986; Philpotts and Dickson, 2000). The absence of evolved plagioclase compositions ($<An_{60}$) in the Upper Border Series of the Sept Iles intrusion clearly indicates that roof cumulate sequence has not developed and thus that nucleation and crystallization at the roof were very subordinate processes.

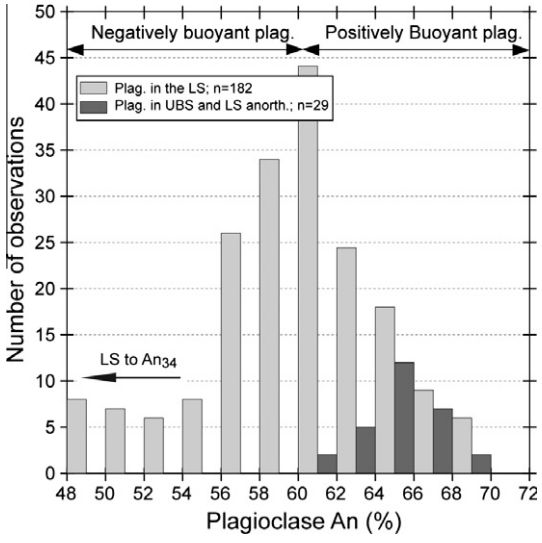

Fig. 12. Histogram showing the range of plagioclase core compositions (An%) observed in the Sept Iles layered intrusion. Plagioclase from the anorthosites ranges from An_{60} to An_{69}, while plagioclase from cumulate rocks of the Layered Series ranges from An_{34} to An_{70}. This diagram illustrates that buoyant plagioclase (An_{60-69}) is present in both anorthosites and floor cumulates of the Layered Series.

The presence of positively buoyant plagioclase both at the floor (Layered Series) and at the roof (Upper Border Series) of the Sept Iles intrusion may be explained by two phenomena: imperfect in situ crystallization mechanism and homogeneous nucleation of a low proportion of crystals in the main magma body. (1) In situ crystallization along the floor of the magma chamber prevents plagioclase flotation by attachment of the crystals to the magma chamber side (Campbell, 1978; McBirney and Noyes, 1979). This process may be assisted by the formation of coherent three-dimensional chains of crystals (Philpotts and Carroll, 1996; Philpotts et al., 1998; Philpotts and Dickson, 2000). However, the in situ crystallization process is generally not fully effective (McBirney and Noyes, 1979) and crystal chains are not entirely consolidated before the proportion of crystals reaches 30% (Philpotts et al., 1998). Consequently, some isolated plagioclase crystals may escape the cotectic assemblage and rise up to the top of the magma chamber to form the anorthosite. This process might also be facilitated by convection currents driving plagioclase grains upwards (e.g. Marsh and Maxey, 1985; Brandeis and Jaupart, 1986; Turner and Campbell, 1986; Marsh, 1988; Higgins and Chandrasekharam, 2007); (2) In situ crystallization can be accompanied by subordinate homogeneous nucleation and crystallization of grains within the main magma body. These grains are isolated and able to float or sink, depending on their relative density to that of the magma (Martin and Nokes, 1988, 1989; Weinstein et al., 1988; Verhoven and Schmalzl, 2009). This process could thus explain the formation of anorthosite even in the case of a fully effective in situ crystallization at the floor of the magma chamber.

In the Sept Iles intrusion, it has been calculated by least-squares regression that the cotectic proportion of plagioclase crystallizing from liquids in equilibrium with troctolite

is 78 wt.% (Namur et al., 2011). This value is slightly higher than that determined for other ferrobasaltic magmas (72–74 wt.%; Toplis and Carroll, 1995; Thy et al., 2006), but is in good agreement with that determined for FeO_t-rich MORB compositions and calc-alkaline lavas of the Medecine Lake Volcano (78 wt.%; Grove et al., 1982, 1992). For Fe–Ti oxide-bearing troctolites, no estimation is available. However, comparison with experimental data suggests a plagioclase cotectic proportion of 60–70 wt.% (Snyder et al., 1993; Vander Auwera and Longhi, 1994). Fig. 13a and b show the modal proportions of plagioclase in troctolites (50.0–79.7 wt.%; average: 67.5 wt.%) and Fe–Ti oxide-bearing troctolites (14.6–69.6 wt.%; average: 50.4 wt.%) of the Layered Series (Namur et al., 2010). Mineral modes from point-counting (vol.%) were converted in wt.% (using the density of the minerals) to allow a more straightforward comparison with cotectic proportions. Plagioclase modes are generally lower than the estimated cotectic proportions, indicating that part of the plagioclase has not accumulated in the Layered Series (Fig. 13a and b). Based on average modes, it can be estimated that 13 wt.% of the plagioclase is missing from basal troctolites, while 16–28 wt.% (depending on the considered cotectic proportion) of the plagioclase is missing from Fe–Ti oxide-bearing cumulates.

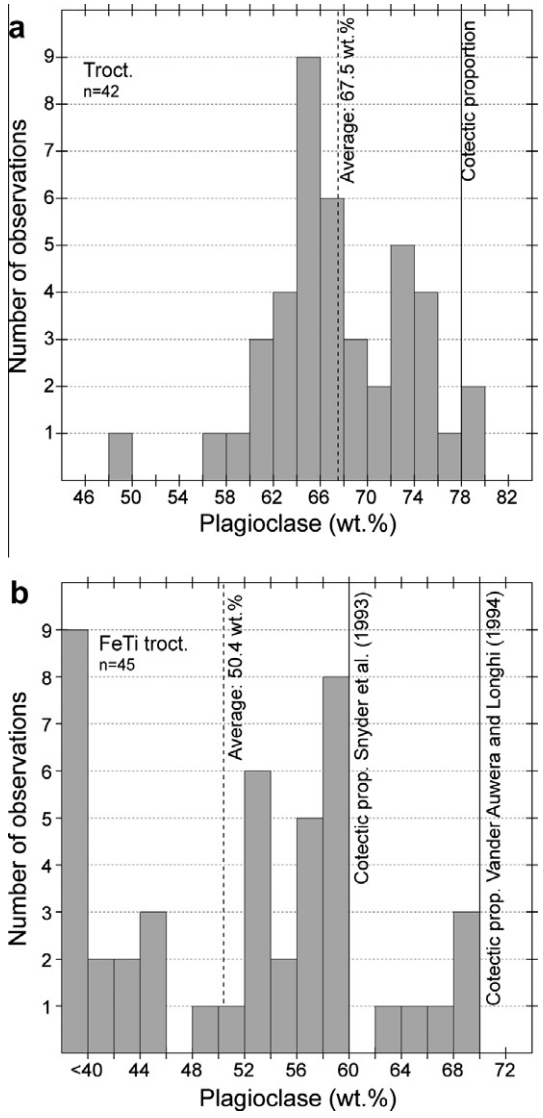

Fig. 13. (a) Modal proportion (wt.%) of plagioclase in troctolites from the Layered Series and comparison with the cotectic proportion of plagioclase calculated by Namur et al. (2011). (b) Modal proportion of plagioclase in Fe–Ti oxide-bearing troctolites and comparison with cotectic proportions determined from the experiments by Snyder et al. (1993) and Vander Auwera and Longhi (1994). Modal data from Namur et al. (2010).

6.2.4. *Mafic minerals in anorthosites*

Due to their high densities, the presence of ferromagnesian and Fe–Ti oxide minerals in the anorthosites cannot result from accumulation of liquidus grains, except in chains with low proportions of Fe–Mg silicate minerals ± Fe–Ti oxide minerals (Philpotts and Dickson, 2000). Alternatively mafic minerals in anorthosites may represent cumulus phases having crystallized against the magma chamber roof. However, this is not supported by (1) experimental studies showing that large aspect-ratio magma chambers mostly crystallize at the floor (Brandeis and Jaupart, 1986; Martin, 1990) and (2) the strong decoupling in the evolution of the anorthite content vs Mg# between anorthosites and basal cumulates (Fig. 7), which is not observed in other intrusions where crystallization simultaneously occurs at the floor and at the roof (e.g. Morse, 1979b; McBirney, 1996). This decoupling suggests different processes of crystallization for the abundant plagioclase compared to the minor mafic minerals.

Here we suggest that mafic minerals in the anorthosites may have crystallized from the interstitial liquid, as already proposed by Raedeke and McCallum (1980). The proportion of interstitial liquid in anorthosites associated with layered intrusions varies between less than 10% (Haskin and Salpas, 1992) to more than 30% (Raedeke and McCallum, 1980; Maier, 1995). Here we used two different approaches to calculate the fraction of trapped interstitial liquid (F_{TL}) in Sept Iles anorthosites, and we note that they give relatively consistent results: (1) we used the whole-rock concentration of an element (P_2O_5) that is highly incompatible in the cumulus phases (see Electronic Annex). Calculations suggest a high F_{TL} (12–64%; average: 32%; Fig. 15; Table EA9); (2) using least-squares regression of whole-rock, plagioclase and liquid compositions, we determined the relative proportion of plagioclase and liquid in each sample, by making the assumption that anorthosites are made up of a mixture of cumulus plagioclase and liquid (see Electronic Annex for details on the calculation procedure). Using this methodology, we calculated high F_{TL} values (13–51%; average: 29%). The two different approaches indicate high F_{TL} in Sept Iles anorthosite rocks, in agreement with the large interstitial rims observed around plagioclase grains. The variable F_{TL} values from one sample to another sample probably result from a process of fluid migration within the crystal mush (McKenzie, 1984; Tait et al., 1984; Morse, 1986; Turner and Campbell, 1986).

Considering the calculated amounts of trapped liquid, mafic minerals in anorthosites may be fully interpreted as interstitial crystals. In addition to these high F_{TL} values

and the distinctively poikilitic texture of these minerals, geochemical characteristics of mafic minerals also constrain their interstitial status: (1) for a given range of plagioclase core compositions (An_{68}–An_{61}), olivine and clinopyroxene in anorthosites have lower Mg# and lower contents in compatible trace elements (Ni and Cr) than the same minerals in cumulate rocks of the Layered Series (Fig. 7). These evolved compositions in anorthosites indicate that clinopyroxene and olivine are in disequilibrium with plagioclase cores; (2) compared to the cumulus clinopyroxene of the gabbros from the Layered Series, the REE patterns of clinopyroxene in anorthosites show strong negative Eu anomalies and high HREE contents (Fig. 8c). Such features are considered as a strong evidence for clinopyroxene crystallization from interstitial melt (Cawthorn, 1996; Hermann et al., 2001). This is confirmed by the strong resemblance between REE patterns of clinopyroxene from anorthosites and those of clinopyroxene from basal troctolites of the Layered Series, for which the interstitial nature has been clearly established on the basis of textural and geochemical arguments (Namur et al., 2010). Most plagioclase rim compositions lie within the An_{68} and An_{63} interval (Fig. 10). In the Layered Series, plagioclase with this range of composition is in equilibrium with olivine $Fo_{60\text{-}67}$ and clinopyroxene $Mg\#_{70\text{–}75}$ (Figs. 7 and 12). These compositions of olivine and clinopyroxene globally correspond to those observed in anorthosites ($Fo_{59\text{–}66}$; Mg#-$cpx_{66\text{–}75}$), thus suggesting that plagioclase rims are in equilibrium with mafic minerals that are thus interpreted as being interstitial phases.

6.2.5. Synthetic model for the distribution of plagioclase in the Sept Iles magma chamber

During the early differentiation of the Sept Iles layered intrusion, the melt density was higher than that of equilibrium plagioclase (Fig. 14a). Some plagioclase grains were thus able to rise up through the magma column to form anorthosite (Upper Border Series) at the roof of the magma chamber (Fig. 14b). The onset of Fe–Ti oxide crystallization caused a drastic decrease of the magma density. When the melt density became lower than ca. 2.65, plagioclase stopped floating and the formation of anorthosite at the top of the magma chamber ceased (Fig. 14b), while cotectic gabbros started to crystallize at the top of the cumulus pile in the Layered Series. In addition, previously formed anorthosite of the Upper Border Series has started to sink as blocks from the roof down to the basal crystal pile. Mafic minerals having crystallized from the interstitial liquid in anorthosites may have also facilitated the sinking of blocks.

6.3. Implications for the lunar crust

6.3.1. Lithologies of the lunar crust

Differentiation of the Moon is interpreted to have resulted initially from the crystallization of a lunar magma ocean (LMO; e.g. Wood et al., 1970; Warren, 1985). The lunar crust is defined by the first appearance of cumulus plagioclase in the cumulate succession (Shearer and Papike, 1999). Seismic data indicate that the thickness of the lunar crust is in the range of 20–120 km, with an average value of 45–60 km (Toksoz et al., 1974; Neumann et al., 1996; Khan et al., 2000; Hikida and Mizutani, 2005; Ishihara et al., 2009).

The lunar crust is mostly composed of rocks resulting from the crystallization of the LMO, with the exception of the mare basalts, rocks from the alkali-suite and rocks from the magnesian suite (Wieczorek et al., 2006). Crustal rocks having crystallized from the LMO were traditionally considered to be highly anorthositic (ferroan anorthosite suite; FAS; Wood et al., 1970). However, a number of evidences now suggest that the lunar crust is vertically stratified with mafic rocks at the base and felsic rocks at the top: (1) a seismic discontinuity occurs at ca. 20 km depth beneath the surface of the Apollo 12 and 14 landing sites. Moreover, the relationship between gravity and density of the Moon suggests a compositional stratification within the crust (Toksoz et al., 1974; Wieczorek and Phillips, 1997); (2) mostly based on Clementine multispectral reflectance data, it was shown that the ejecta of large basins, the central peaks of some craters and the South Pole-Aitken basin are more mafic (mostly noritic) than the surrounding anorthositic highlands (e.g. Lucey et al., 1995; Spudis et al., 1996; Pieters et al., 1997; Wieczorek and Phillips, 1998; Tompkins and Pieters, 1999; Bussey and Spudis, 2000; Hawke et al., 2003; Cahill et al., 2009).

Wieczorek and Zuber (2001) have investigated the mineralogy of the lunar lower crust based on Clementine spectral data collected in crater central peaks. Based on 6 craters that expose deep material, these authors concluded that the lower crust is mafic (norite, gabbronorite, anorthositic norite; 65 ± 8 vol.% of plagioclase). The mafic nature of the lower crust was also recently confirmed by radiative transfer modeling of impact central peak craters (Cahill et al., 2009). By contrast, mineralogical data from Clementine, SELENE and detailed analysis of Apollo FAS rocks and meteorites indicate that the upper crust is highly enriched in plagioclase (82–100 vol.%; Warren, 1990, 2005; Palme et al., 1991; Lucey et al., 1998; Tompkins and Pieters, 1999; Korotev, 2000; Wieczorek and Zuber, 2001; Korotev et al., 2003, 2010; Warren et al., 2005; Ohtake et al., 2009).

6.3.2. Lunar rocks and LMO crystallization

Based on different estimates of the LMO composition (e.g. Taylor, 1982; O'Neill, 1991), it has been proposed that plagioclase saturated after 68–78% of dunite and orthopyroxenite fractionation, whereas ilmenite saturated after 95% crystallization (Snyder et al., 1992; Longhi, 2003). Fractionation of ilmenite-free cumulates was responsible for an increase of the melt FeO_t-content to 14–15 wt.% at the appearance of plagioclase and to 22 wt.% at the appearance of ilmenite (Warren, 1990; Longhi, 2003). Warren (1990) estimated that the density of residual melts of the LMO (Fig. 14c) increased with fractionation from 2.69 to 2.72 g/cm^3 at $F = 100\%$ to 2.80–2.84 g/cm^3 ($F = 22\%$) and 2.88–2.92 g/cm^3 ($F = 5\%$). Crystallization of ilmenite-bearing gabbro-norite was then responsible for a decrease of the melt FeO_t-content and the melt density, but the exact evolution is unknown (Fig. 14c).

The formation of the anorthosite lunar crust was traditionally interpreted as resulting from the separation of

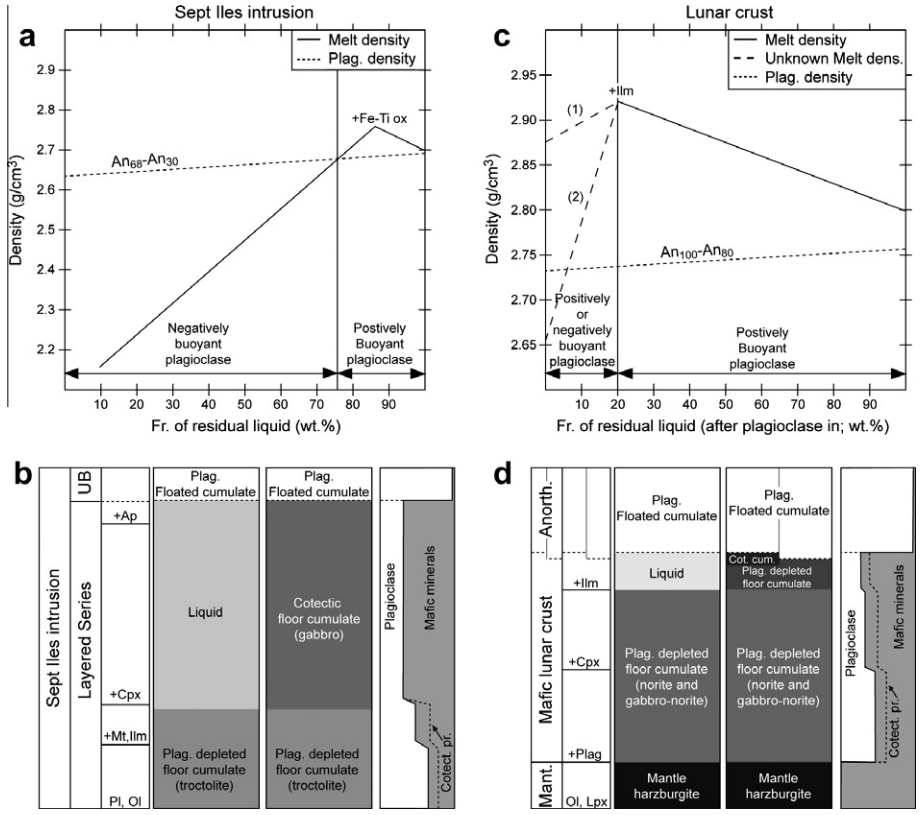

Fig. 14. Schematic models for the distribution of plagioclase in the Sept Iles intrusion and in the lunar crust. (a) Evolution of Sept Iles plagioclase and liquid densities as a function of the proportion of residual liquid. (b) Simplified stratigraphic column of the Sept Iles intrusion showing the sequence of cumulus phases, the mechanisms of crystallization and the relative proportions of plagioclase and mafic minerals. Troctolite and Fe–Ti oxide-bearing troctolite crystallize in situ on the floor of the magma chamber. Part of the plagioclase grains floats to the top of the magma chamber where they accumulate to form a 100–500 m-thick anorthosite (Upper Border Series). Just before the saturation of clinopyroxene, the density of the magma becomes lower than that of equilibrium plagioclase, which is therefore no longer buoyant. Cotectic gabbro thus crystallizes in situ on the top of the previously formed troctolite crystal pile. (c) Evolution of crustal lunar magmas and plagioclase (An_{100-80}) densities as a function of the proportion of residual liquid in the LMO after the appearance of cumulus plagioclase. The sequence of crystallization is after Snyder et al. (1992) and Longhi (2003). The evolution of magma density (until the saturation of ilmenite) is after Warren (1990). Crystallization of ilmenite-free norite and gabbro-norite results in an increase of the magma density. After the saturation of ilmenite, the evolution of magma density is unknown and two possibilities are envisaged: (1) The density of the magma decreases slightly but remains higher than the density of plagioclase until $F = 0\%$; (2) the magma density decreases rapidly and becomes lower than that of equilibrium plagioclase before $F = 0\%$. As a consequence, plagioclase is buoyant before the saturation of ilmenite but becomes non-buoyant rapidly after ilmenite saturation. (d) Stratigraphic column of the lunar crust and proposed mechanisms of crystallization with resulting relative proportions of plagioclase and mafic minerals. Norite and gabbro-norite crystallize in situ at the top of the previously formed mantle crystal pile. Part of the plagioclase grains ascends to the top of the LMO to form anorthosite (FAS). Plagioclase may also float during the crystallization of ilmenite-bearing gabbro-norite. However, if the density of the liquids is lower than that of equilibrium plagioclase, cotectic ilmenite-bearing cumulate crystallizes and the formation of the FAS ends.

plagioclase, floating to the top of the LMO, while mafic minerals sink to the top of the previously crystallized mantle cumulates (Wood et al., 1970; Taylor, 1982; Warren, 1985, 1990; Snyder et al., 1992). This widely accepted model was however challenged by the recent compositionally layered model of the lunar crust indicating that rocks with a proportion of plagioclase up to 50 wt.% occur in the lower and middle parts of the lunar crust (Wieczorek and Zuber, 2001; Cahill et al., 2009).

Wieczorek and Zuber (2001) suggested that all parts of the lunar crust could have been formed by cotectic cumulate flotation on LMO magmas. There are however several lines of evidence making this argument untenable: (1) average estimated densities of the lower crust range from 2.94 to 3.04 g/cm^3 (Wieczorek and Zuber, 2001) and are higher than the highest liquid density of the LMO (Warren, 1990; Fig. 14c); (2) it has been calculated that cotectic assemblages with only 69–80 wt.% of plagioclase (ca. 2.88–2.92 g/cm^3) may float on LMO magmas (Warren, 1990; Wieczorek and Zuber, 2001; Warren et al., 2005). These estimates cannot explain the presence of norite (50 vol.% of plagioclase; density: 3.00–3.20 g/cm^3) in the lower crust and ilmenite-bearing norite (3.40–3.80 g/cm^3; Elkins Tanton et al., 2002) in the middle crust.

6.3.3. Model for the stratigraphy of the lunar crust

Processes related to floating and sinking of plagioclase in the Sept Iles intrusion might contribute to a better under-

standing of the stratigraphy of the lunar crust. We suggest that the mafic lower crust (norite and gabbro-norite) has crystallized in situ at the base of the LMO on the previously formed crystal pile, represented by ultramafic mantle rocks (Fig. 14d). During crystallization of norite and gabbro-norite in the lower crust, plagioclase formed three-dimensional coherent chains that enclose ferromagnesian minerals ± ilmenite. These cotectic networks were denser than magmas from the LMO and prevented cumulate rock flotation. However, as shown for Sept Iles, some isolated plagioclase grains may have escaped the networks and floated to the top of the LMO to form the FAS (Fig. 14d). The density contrast between plagioclase grains and the equilibrium melts is higher during LMO crystallization compared to the Sept Iles intrusion. However, the gravitational attraction on the Moon is only one-sixth the terrestrial value and thus, the efficiency of plagioclase flotation is probably relatively similar in both cases. Considering the estimation of LMO differentiation path by Snyder et al. (1992) and the efficiency of plagioclase flotation observed for the Sept Iles intrusion (up to 30%), plagioclase accumulation at the top of the LMO allows the formation of a ca. 8 km-thick anorthosite layer. This thickness is slightly higher than the estimation of Longhi (1982) but lower than the 15–20 km thickness suggested by most authors (e.g. Wood, 1986; Ohtake et al., 2009). The calculated thickness of pure anorthosite produced by flotation of plagioclase grains may however be underestimated because: (1) the cotectic proportion of plagioclase (53% before the saturation of clinopyroxene and 31% after clinopyroxene in) calculated by Snyder et al. (1992) is relatively low compared to those observed for troctolitic magmas on Earth (Morse et al., 2004). Cotectic proportions similar to those observed on Earth would allow the formation of an anorthosite layer thicker than 10 km; (2) the thickness of the lunar crust is generally thought to range between 60 and 120 km (e.g. Neumann et al., 1996; Chenet et al., 2006; Wieczorek, 2009). Changing the lunar crust thickness by a factor 2 would also change the resulting thickness of pure anorthosite by the same factor.

After the saturation of ilmenite in the LMO, the density of residual liquids decreased significantly. The exact path being unknown, two different ways for forming the lunar crust exist: (1) if ilmenite saturated melts were denser than plagioclase (ca. $An_{80–60}$; 2.73 g/cm^3), some plagioclase grains continued floating, thus contributing to the formation of the FAS and increasing the total thickness of the anorthosite layer (Fig. 14d); (2) if ilmenite-saturated melts were less dense than plagioclase, the formation of the FAS ended. In this case, previously formed FAS-rocks may have sunk as blocks into ilmenite-saturated melts from the lunar surface to the top of the crystal pile. This process could potentially explain the presence of highly anorthositic rocks at different levels of the lunar crust, even between mafic cumulate layers of the middle crust (Wieczorek and Zuber, 2001; Cahill et al., 2009).

6.3.4. Mafic minerals in lunar anorthosites

Considering the number of samples available for ferroan anorthosites, their size, possible polymictic origin, cataclasis and recrystallization (James et al., 1989, 1991), the cumulus origin of ferromagnesian minerals (olivine, pigeonite and clinopyroxene) may be at best postulated (Longhi, 1982, 2003; Wieczorek et al., 2006). However, several lines of evidence make this hypothesis questionable: (1) mafic minerals in anorthosite rocks frequently display a very clear poikilitic texture (James et al., 1989; Warren, 1990), which is traditionally interpreted as a strong evidence for crystallization from the interstitial liquid in the pore space; (2) mafic minerals in FAS rocks from the Apollo missions (pristine index >7; Warren, 1993) show a large compositional range at a given plagioclase An-content (e.g. $An_{96±1}$; orthopyroxene $Mg\#_{44–73}$; olivine $Fo_{50–74}$), indicating that at least some grains are in disequilibrium with associated plagioclase cores; (3) the most iron-rich compositions of ferromagnesian minerals in FAS ($Mg\#_{33–62}$; Goodrich et al., 1984; Warren, 1993) cannot have crystallized in equilibrium with highly An-rich plagioclase ($An_{94–97}$; Floss et al., 1998), except from a liquid with an alkali-content approaching zero (Longhi, 1982). However, even in this case, formation of mafic minerals by fractional crystallization cannot explain the absence of primitive compositions (Mg# > 60).

A more straightforward explanation for the presence and the iron-rich composition of ferromagnesian minerals would be a direct crystallization from the interstitial liquid, as observed in anorthosites of the Sept Iles layered intrusion. The mafic mineral-content in Sept Iles anorthosites is between 3% and 20%, thus covering the whole range observed in the lunar anorthosites (Korotev et al., 2003). The variable amount of mafic minerals in Sept Iles anorthosites is explained by a non-uniform distribution of the interstitial liquid (10–50%), due to convection within the anorthosite mush (Tait et al., 1984; Morse, 1986). A similar model may be proposed for the lunar crust where anorthosite is formed by flotation atop a convecting magma ocean (Herbert et al., 1977; Morse, 1982, 1987; Solomatov, 2000; Loper and Werner, 2002). This hypothesis of crystallization of the mafic minerals from the interstitial liquid is reasonable in light of the trapped liquid-content determined for lunar soils of the Apollo 16 landing site (30%; Jolliff and Haskin, 1995).

6.3.5. Potential geochemical characteristics of the lunar lower crust

Recent interpretations from Clementine data together with mineral modes from lunar meteorites give further insight on the vertically stratified nature of the lunar crust. The distribution of mineral modes within the lunar crust is remarkably similar to that observed in floor and roof cumulates of the Sept Iles layered intrusion (Fig. 15). This similarity allows us to make assumptions on the geochemical characteristics of the lunar lower crust, mainly for mineral compositions that are mostly unknown. Based on crystallization mechanisms observed in the Sept Iles Layered Series, it is suggested that plagioclase and mafic minerals in the lunar lower crust may have followed a normal trend of fractional crystallization of the LMO. The plagioclase An-content should slightly decrease bottom-up together with a more pronounced decrease of the Mg# of ferromagnesian minerals. It is moreover suggested that ma-

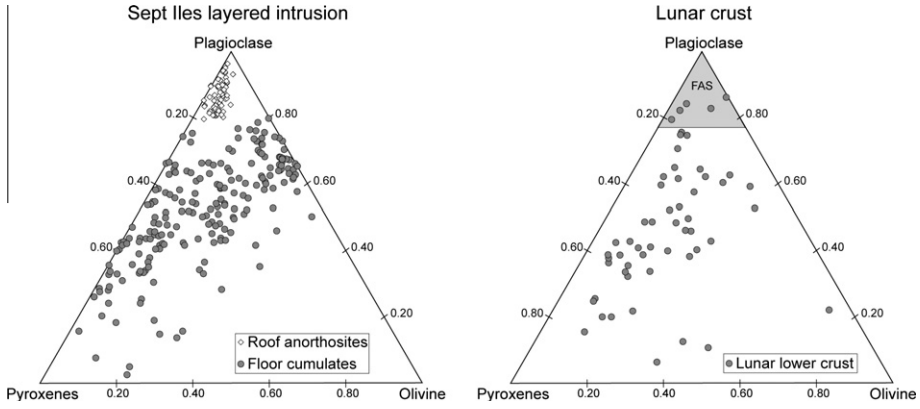

Fig. 15. Comparison between mineral modes (plagioclase, olivine and pyroxenes) in the Sept Iles layered intrusion and in the lunar crust. Left Sept Iles intrusion. Data from the floor cumulates are from Namur et al. (2010). Right Lunar crust. Data for the FAS have been calculated from the whole-rock Al_2O_3 content of meteorites reported in Korotev et al. (2003). Data for the lunar lower crust are from Cahill et al. (2009).

fic minerals at the basis of the lunar crust should have Mg# values significantly higher than those observed in FAS rocks. A significant decoupling in the evolution of mafic mineral compositions (Mg#) as a function of plagioclase composition (An-content) is thus expected between FAS rocks and rocks from the lunar lower crust. This kind of decoupling is well known to occur between mineral compositions from FAS rocks and rocks from the magnesian-suite (troctolite, norite, gabbro; Warren, 1993). However, most magnesian-suite rocks are enriched in a KREEP component, considered as representing residual liquids of the LMO (e.g. Shearer and Papike, 2005), which cannot be explained by a fractional crystallization model similar to that of the Sept Iles Layered Series. However, it has been suggested that two kinds of magnesian suite may exist in the lunar crust, one being enriched in KREEP component and which could potentially be restricted to the Procellarum and Imbrium basins (Metzberg et al., 1973; Lawrence et al., 1998, 2000; Jolliff et al., 2000) and the other one being free of KREEP component (Longhi and Boudreau, 1979; Korotev, 2005). Based on the Sept Iles model, we suggest that the rocks from the two magnesian-suites would have been produced by fractional crystallization of magmas that have different origins: the LMO for the KREEP-free suite and a KREEP-contaminated magma for the other suite. The origin of the latter magma has been extensively discussed in the literature (Warren, 1986; Hess, 1994; Shearer and Papike, 2005; Longhi, 2009). Crystallization of these magmas would produce rocks with relatively similar evolutions of major element mineral compositions but contrasted whole-rock concentrations for incompatible trace elements (e.g. Th).

7. CONCLUSIONS

Anorthosite cumulates have been recognized in many layered intrusions (e.g. Bushveld; Cawthorn and Ashwal, 2009; Stillwater; Haskin and Salpas, 1992; Duluth; Miller and Weiblen, 1990), but Sept Iles is the only known example of a layered intrusion exposing a thick anorthosite layer at its roof.

Density calculation of plagioclase and liquid along the Sept Iles liquid line of descent suggests that plagioclase was positively buoyant on primitive basaltic melts during the early differentiation of the intrusion, but that the flotation ability disappeared soon after saturation of Fe–Ti oxides. The calculated compositional range of the positively buoyant plagioclase (An_{69}–An_{60}) is identical to that observed in anorthosites forming the top of the intrusion (Upper Border Series). Therefore, we propose that these anorthosites were formed by accumulation of floated plagioclase grains which have initially crystallized at the bottom (Layered Series) of the Sept Iles intrusion. However, the presence of An_{69}–An_{60} plagioclase in the Layered Series indicates that the ability of plagioclase to float was moderate. Minor nucleation from the main magma body and plagioclase flotation to the top of the magma chamber is also envisaged as a possible mechanism for the Sept Iles anorthosite formation. After saturation of the Fe–Ti oxides in the main magma body, the melt density decreased below that of plagioclase and blocks of anorthosite (autoliths) started to sink from the roof of the intrusion down to the top of the crystal pile in the Layered Series. Ferromagnesian minerals and Fe–Ti oxides in the Sept Iles anorthosites have probably crystallized from the interstitial melt, as suggested by their evolved compositions.

Magma chamber processes occurring in the Sept Iles intrusion are used as a proxy to explain stratigraphic features observed in the lunar crust crystallized from the lunar magma ocean (LMO). We suggest that the mostly noritic lower crust may result from in situ fractional crystallization at the base of the lunar magma ocean, while ferroan anorthosites occurring in the upper crust may have been formed by plagioclase flotation in melts of the LMO. The presence of plagioclase in the lower crust is interpreted as resulting from the low efficiency of plagioclase to escape the basal cumulates or from the low amount of crystals nucleating from the main magma body of the LMO. Finally, mineralogical data from the Sept Iles Layered Series lead us to suggest that ferromagnesian minerals at the base of the lunar lower crust may be more primitive than those observed in FAS rocks. This geochemical signature would be similar

to rocks of the magnesian-suite that do not contain a KREEP-signature. Our crystallization model for the lunar crust thus supports the idea that two magnesian-suites may exist within the lunar crust (Longhi and Boudreau, 1979; Korotev, 2005).

ACKNOWLEDGMENTS

This work was financed by the Belgian Fund for Joint Research (FNRS). B.C. acknowledges support by a Marie Curie International Outgoing Fellowship within the 7th European Community Framework Programme. The Ministère des Ressources Naturelles et de la Faune du Québec and the Soquem Company are gratefully acknowledged for giving access to the drill-cores. M.D. Higgins is thanked for his help during fieldwork and for his precious expertise on the Sept Iles intrusion. J.L. Devidal, G. Bologne, C. Gilson and C. Allen are thanked for assistance with geochemical analyses. Discussions with A.R. McBirney, I.V. Veksler, R. Latypov, H. St. C. O'Neill, M.J. Toplis, M.B. Holness and R.G. Cawthorn, and comments by J.C. Duchesne, C. Tegner and T.L. Grove were greatly appreciated. S.A. Morse, J. Longhi and D. Walker are greatly acknowledged for their very constructive and detailed reviews that highly improved the quality of the manuscript. R. Korotev is also thanked for detailed comments and editorial handling. M.B. Holness (University of Cambridge, UK) is greatly acknowledged for giving to ON the time to complete this contribution.

APPENDIX A. SUPPLEMENTARY DATA

Supplementary data associated with this article can be found, in the online version, at doi:10.1016/j.gca.2011.06.013.

REFERENCES

Ashwal L. D. (1993) *Anorthosites Minerals and Rocks*. Springer, Berlin, p. 422.

Batiza R. and Niu Y. (1992) Petrology and magma chamber processes at the East Pacific Rise ~ 9°30′N. *J. Geophys. Res.* **97**, 6779–6797.

Blewett D. T., Robinson M. S., Denevi B. W., Gillis-Davis J. J., Head J. W., Solomon S. C., Holsclaw G. M. and McClintock W. E. (2009) Multispectral images of Mercury from the first MESSENGER flyby: analysis of global and regional color trends. *Earth Planet. Sci. Lett.* **285**, 272–282.

Bogaerts M., Scaillet B. and Vander Auwera J. (2006) Phase equilibria of the Lyngdal granodiorite (Norway): implications for the origin of metaluminous ferroan granitoids. *J. Petrol.* **47**, 2405–2431.

Bottinga Y. and Weill D. F. (1970) Densities of liquid silicate systems calculated from partial molar volumes of oxide components. *Am. J. Sci.* **269**, 169–182.

Brandeis G., Jaupart C. and Allègre C. J. (1984) Nucleation crystal growth and the thermal regime of cooling magmas. *J. Geophys. Res.* **89**, 10161–10177.

Brandeis G. and Jaupart C. (1986) On the interaction between convection and crystallization in cooling magma chambers. *Earth Planet. Sci. Lett.* **77**, 345–361.

Brown S. M. and Elkins-Tanton L. T. (2009) Compositions of Mercury's earliest crust from magma ocean models. *Earth Planet. Sci. Lett.* **286**, 446–455.

Bussey D. B. and Spudis P. D. (2000) Compositional studies of the Orientale, Humorum Nectaris and Crisium lunar basins. *J. Geophys. Res.* **105**, 4235–4243.

Cahill J. T., Lucey P. G. and Wieczorek M. A. (2009) Compositional variations of the lunar crust: results from radiative transfer modelling of central peak spectra. *J. Geophys. Res.* **114**, E09001.

Campbell I. H. (1978) Some problems with the cumulus theory. *Lithos* **11**, 311–323.

Campbell I. H. (1996) Fluid dynamic processes in basaltic magma chambers. In *Layered Intrusions Developments in Petrology* (ed. R. G. Cawthorn). Elsevier, Amsterdam, pp. 45–76.

Campbell I. H., Roeder P. L. and Dixon J. M. (1978) Plagioclase buoyancy in basaltic liquids as determined with a centrifuge furnace. *Contrib. Mineral. Petrol.* **67**, 369–377.

Cawthorn R. G. (1996) Models for incompatible trace-element abundances in cumulus minerals and their application to plagioclase and pyroxenes in the Bushveld Complex. *Contrib. Mineral. Petrol.* **123**, 109–115.

Cawthorn R. G. and Ashwal L. D. (2009) Origin of anorthosite and magnetitite layers in the Bushveld Complex constrained by major element compositions of plagioclase. *J. Petrol.* **50**, 1607–1637.

Charlier B., Duchesne J. C., Vander Auwera J., Storme J. Y., Maquil R. and Longhi J. (2010) Polybaric fractional crystallization of high-alumina basalt parental magmas in the Egersund-Ogna massif-type anorthosite (Rogaland, SW Norway) constrained by plagioclase and high-alumina orthopyroxene megacrysts. *J. Petrol.* **51**, 2515–2546.

Chenet H., Lognonné P., Wieczorek M. A. and Mizutani H. (2006) Lateral variations of the lunar crustal thickness from the Apollo seismic data set. *Earth Planet. Sci. Lett.* **243**, 1–14.

Dall'Agnol R., Scaillet B. and Pichavant M. (1999) An experimental study of a lower Proterozoic A-type granite from the Eastern Amazonian Craton Brazil. *J. Petrol.* **40**, 1673–1698.

Duchesne J. C., Liégeois J. P., Vander Auwera J. and Longhi J. (1999) The crustal tongue melting model and the origin of massive anorthosites. *Terra Nova* **11**, 100–105.

Elkins Tanton L. T., Van Orman J. A., Hager B. H. and Grove T. L. (2002) Re-examination of the lunar magma ocean cumulate overturn hypothesis: melting or mixing is required. *Earth Planet. Sci. Lett.* **196**, 239–249.

Elthon D. (1984) Plagioclase buoyancy in oceanic basalts: chemical effects. *Geochim. Cosmochim. Acta* **48**, 753–768.

Emslie R. F. (1985) Proterozoic anorthosite massifs. In *The Deep Proterozoic Crust in the North Atlantic Provinces NATO ASI C158* (eds. A. C. Tobi and J. L. Touret). Kluwer Academic, Dordrecht, pp. 39–60.

Floss C., James O. B., McGee J. J. and Crozaz G. (1998) Lunar ferroan anorthosite petrogenesis: clues from trace element distributions in FAS subgroups. *Geochim. Cosmochim. Acta* **62**, 1255–1283.

Flower M. F. (1980) Accumulation of calcic plagioclase in ocean-ridge tholeiite: an indication of spreading rate. *Nature* **287**, 530–532.

Forst B. R. and Lindsley D. H. (1992) Equilibria among Fe–Ti oxides pyroxenes olivine and quartz. Part II: Application. *Am. Mineral.* **77**, 1004–1020.

Goodrich C. A., Taylor G. J., Keil K., Boynton W. V. and Hill D. H. (1984) Petrology and chemistry of hyperferroan anorthosites and other clasts from lunar meteorite ALHA81005. *J. Geophys. Res.* **89**, 87–94.

Grove T. L., Gerlach D. C. and Sando T. W. (1982) Origin of calc-alkaline series lavas at Medicine Lake Volcano by fractionation assimilation and mixing. *Contrib. Mineral. Petrol.* **80**, 160–182.

Grove T. L., Kinzler R. J. and Bryan W. B. (1992) Fractionation of mid-ocean ridge basalt (MORB). In *Mantle Flow and Melt Generation at Mid-ocean Ridges* (eds. J. Phipps-Morgan, D. K. Blackman and J. M. Sinton). American Geophysical Union, pp. 281–310.

Haskin L. A. and Salpas P. A. (1992) Genesis of compositional characteristics of Stillwater An-I and An-II thick anorthosite units. *Geochim. Cosmochim. Acta* **56**, 1187–1212.

Hawke B. R., Peterson C. A., Blewett D. T., Bussey D. B., Lucey P. G., Taylor G. J. and Spudis P. D. (2003) Distribution and modes of occurrence of lunar anorthosite. *J. Geophys. Res.* **108**, 5050.

Herbert F., Drake M. J., Sonett C. P. and Wiskerchen M. (1977) Some constraints on the thermal history of the lunar magma ocean. *Lunar Planet. Sci. VIII. Lunar Planet. Inst., Houston*, 573–582.

Hermann J., Müntener O. and Günther D. (2001) Differentiation of mafic magma in a continental crust-to-mantle transition zone. *J. Petrol.* **42**, 189–206.

Hess P. C. (1994) Petrogenesis of lunar troctolites. *J. Geophys. Res.* **99**, 19083–19093.

Higgins M. D. (1991) The origin of laminated and massive anorthosite Sept Iles layered intrusion Québec Canada. *Contrib. Mineral. Petrol.* **106**, 340–354.

Higgins M. D. (2005) A new interpretation of the structure of the Sept Iles Intrusive Suite Canada. *Lithos* **83**, 199–213.

Higgins M. D. and Doig R. (1986) Geochemical constraints on the processes that were active in the Sept Iles complex. *Can. J. Earth Sci.* **23**, 670–681.

Higgins M. D. and van Breemen O. (1998) The age of the Sept Iles layered mafic intrusion Canada: implications for the late Neoproterozoic/Cambrian history of southeastern Canada. *J. Geol.* **106**, 421–431.

Higgins M. D. and Chandrasekharam D. (2007) Nature of sub-volcanic magma chambers Deccan Province India: evidence from quantitative textural analysis of plagioclase megacrysts in the Giant Plagioclase Basalts. *J. Petrol.* **48**, 885–900.

Hikida H. and Mizutani H. (2005) Mass and movement of inertia constraints on the lunar crust thickness: relations between crustal density, mantle density and the reference radius of the crust-mantle boundary. *Earth Planet. Space* **57**, 1121–1126.

Hoover J. D. (1989) The chilled marginal gabbro and other contact rocks of the Skaergaard intrusion. *J. Petrol.* **30**, 441–476.

Hunter R. H. and Sparks R. S. (1987) The differentiation of the Skaergaard intrusion. *Contrib. Mineral. Petrol.* **95**, 451–461.

Huppert H. E. and Sparks R. S. (1980) The fluid dynamics of a basaltic magma chamber replenished by influx of hot, dense ultrabasic magma. *Contrib. Mineral. Petrol.* **75**, 279–289.

Irvine T. N. (1970) Heat transfer during solidification of layered intrusions. I: Sheets and sills. *Can. J. Earth Sci.* **7**, 1031–1061.

Irvine T. N., Andersen J. C. and Brooks C. K. (1998) Included blocks (and blocks within blocks) in the Skaergaard intrusion: geological relations and the origins of rhythmic modally graded layers. *Geol. Soc. Am. Bull.* **110**, 1398–1447.

Ishihara Y., Goossens S., Matsumoto K., Noda H., Araki H., Namiki N., Hanada H., Iwata T., Tazawa S. and Sasaki S. (2009) Crustal thickness of the Moon: implications for farside basin structures. *Geophys. Res. Lett.* **36**, L19202.

Jakobsen J. K., Tegner C., Brooks C. K., Kent A. J., Lesher C. E., Nielsen T. F. and Wiedenbeck M. (2010) Parental magma of the Skaergaard intrusion: constraints from melt inclusions in primitive troctolite blocks and FG-1 dykes. *Contrib. Mineral. Petrol.* **159**, 61–79.

James O. B., Lindstrom M. M. and McGee J. J. (1991) Lunar ferroan anorthosite 60025: petrology and chemistry of mafic lithologies. *Proc. Lunar Planet. Sci.* **21**, 63–87.

James O. B., Lindstrom M. M. and Flohr M. K. (1989) Ferroan anorthosite from lunar breccia 64435: implications for the origin and history of lunar ferroan anorthosites. *Proc. Lunar Planet. Sci.* **19**, 219–243.

Jolliff B. L. and Haskin L. A. (1995) Cogenetic rock fragments from a lunar soil: evidence of a ferroan noritic-anorthosite pluton on the moon. *Geochim. Cosmochim. Acta* **59**, 2345–2374.

Jolliff B. L., Gillis J. J., Haskin L. A., Korotev R. L. and Wieczorek M. A. (2000) Major lunar crustal terranes: surface expressions and crustal-mantle origins. *J. Geophys. Res.* **105**, 4197–4416.

Kerr R. C., Woods A. W., Worster M. G. and Huppert H. E. (1990) Solidification of an alloy cooled from above Part 3: Compositional stratification within the solid. *J. Fluid. Mech.* **218**, 337–354.

Khan A., Mosegaard K. and Rasmussen K. L. (2000) A new seismic velocity model for the Moon from a Monte Carlo inversion of the Apollo lunar seismic data. *Geophys. Res. Lett.* **27**, 1591–1594.

Klimm K., Holtz F., Johannes W. and King P. L. (2003) Fractionation of metaluminous A-type granites: an experimental study of the Wangrah Suite Lachlan Fold Belt Australia. *Precambrian Res.* **124**, 327–341.

Korotev R. L. (2000) The great lunar hot spot and the composition and origin of the Apollo mafic ("LKFM") impact-melt breccias. *J. Geophys. Res.* **105**, 4317–4345.

Korotev R. L. (2005) Lunar geochemistry as told by lunar meteorites. *Chem. Erde* **65**, 297–346.

Korotev R. L., Jolliff B. L., Zeigler R. A., Gillis J. J. and Haskin L. A. (2003) Feldspathic lunar meteorites and their implications for compositional remote sensing of the lunar surface and the composition of the lunar crust. *Geochim. Cosmochim. Acta* **67**, 4895–4923.

Korotev R. L., Jolliff B. L. and Zeigler R. A. (2010) On the origin of the Moon's feldspathic highlands, pure anorthosite, and the feldspathic meteorites. *Lunar Planet. Sci. XLI*. Lunar Planet. Inst., Houston. #1440 (abstr.).

Kress V. C. and Carmichael I. S. (1991) The compressibility of silicate liquids containing Fe_2O_3 and the effect of composition, temperature oxygen fugacity and pressure on their redox states. *Contrib. Mineral. Petrol.* **108**, 82–92.

Kushiro I. and Fuji T. (1977) Floatation of plagioclase in magma at high pressures and its bearing on the origin of anorthosite. *Proc. Japan Acad.* **53**, 262–266.

Lange R. A. (1997) A revised model for the density and thermal expansivity of K_2O–Na_2O–CaO–MgO–Al_2O_3–SiO_2 liquids from 700 to 1900 K: extension to crustal magmatic temperatures. *Contrib. Mineral. Petrol.* **130**, 1–11.

Lange R. A. and Carmichael I. S. (1987) Densities of Na_2O–K_2O–CaO–FeO–Fe_2O_3–Al_2O_3–TiO_2–SiO_2 liquids New measurements and derived partial molar properties. *Geochim. Cosmochim. Acta* **51**, 2931–2946.

Latypov R. M. (2003) The origin of marginal compositional reversals in basic–ultrabasic sills and layered intrusions by Soret fractionation. *J. Petrol.* **44**, 1579–1618.

Lawrence D. J., Feldman W. C., Barraclough B. L., Binder A. B., Elphic R. C., Maurice S. and Thomsen D. R. (1998) Global elemental maps of the Moon: the Lunar Prospector gamma-ray spectrometer. *Science* **281**, 1484–1489.

Lawrence D. J., Feldman W. C., Barraclough B. L., Binder A. B., Elphic R. C., Maurice S., Miller M. C. and Prettyman T. H. (2000) Thorium abundances on the lunar surface. *J. Geophys. Res.* **105**, 20307–20331.

Loncarevic B. D., Feininger T. and Lefevre D. (1990) The Sept Iles layered mafic intrusion: geophysical expression. *Can. J. Earth Sci.* **27**, 501–512.

Longhi J. (1982) Effects of fractional crystallization and cumulus processes on mineral composition trends of some lunar and terrestrial rock series. *Lunar Planet. Sci. XIII*. Lunar Planet. Inst., Houston. 54–64.

Longhi J. (2003) A new view of lunar anorthosites: postmagma ocean petrogenesis. *J. Geophys. Res.* **108**, 5083.

Longhi J. (2009) Origin of the magnesian suite cumulates. *Lunar Planet. Sci. XL*. Lunar Planet. Inst., Houston. #2356 (abstr.).

Longhi J. and Ashwal L. D. (1985) Two-stage models for lunar and terrestrial anorthosites: petrogenesis without a magma ocean. *J. Geophys. Res.* **90**, 571–584.

Longhi J., Boudreau A. E. (1979) Complex igneous processes and the formation of the primitive lunar crustal rocks. *Lunar Planet. Sci. X*. Lunar Planet. Inst., Houston. 2085–2105.

Longhi J., Vander Auwera J., Fram M. S. and Monthieth J. N. (1993) Pressure effects kinetics and rheology of anorthositic and related magmas. *Am. Mineral.* **78**, 1016–1030.

Longhi J., Vander Auwera J., Fram M. S. and Duchesne J. C. (1999) Some phase equilibrium constraints on the origin of Proterozoic (Massif) anorthosites and related rocks. *J. Petrol.* **40**, 339–362.

Loper D. E. and Werner C. L. (2002) On lunar asymmetries 1 Tilted convection and crustal asymmetry. *J. Geophys. Res.* **107**, 5046.

Lucey P. G., Taylor G. J. and Malaret E. (1995) Abundance and distribution of iron on the Moon. *Science* **268**, 1150–1153.

Lucey P. G., Blewett D. T. and Hawke B. R. (1998) Mapping of FeO and TiO_2 content of the lunar surface with multispectral imagery. *J. Geophys. Res.* **103**, 3679–3699.

Maier W. D. (1995) Olivine oikocrysts in Bushveld anorthosite: some implications for cumulate formation. *Can. Mineral.* **33**, 1011–1022.

Marsh B. D. (1988) Crystal capture, sorting, and retention in convecting magma. *GSA Bull.* **100**, 1720–1737.

Marsh B. D. and Maxey M. R. (1985) On the distribution and separation of crystals in convecting magma. *J. Volcanol. Geotherm. Res.* **24**, 95–150.

Martin D. (1990) Crystal settling and in situ crystallization in aqueous solutions and magma chambers. *Earth Planet. Sci. Lett.* **96**, 336–348.

Martin D., Griffiths R. W. and Campbell I. H. (1987) Compositional and thermal convection in magma chambers. *Contrib. Mineral. Petrol.* **96**, 465–475.

Martin D. and Nokes R. (1988) Crystal settling in a vigorously convecting magma chamber. *Nature* **332**, 534–536.

Martin D. and Nokes R. (1989) A fluid-dynamical study of crystal settling in convecting magmas. *J. Petrol.* **30**, 1471–1500.

McBirney A. R. (1996) The Skaergaard Intrusion. In *Layered Intrusions Developments in Petrology* (ed. R. G. Cawthorn). Elsevier, Amsterdam, pp. 147–180.

McBirney A. R. and Noyes R. M. (1979) Crystallization and layering of the Skaergaard intrusion. *J. Petrol.* **20**, 487–554.

McKenzie D. (1984) The generation and compaction of partially molten rocks. *J. Petrol.* **25**, 713–765.

Metzberg A. E., Trombka J. I., Peterson L. E., Reedy R. C. and Arnold J. R. (1973) Lunar surface radioactivity: preliminary results of the Apollo 15 and Apollo 16 gamma ray spectrometer experiments. *Science* **179**, 800–803.

Miller J. D. and Weiblen P. W. (1990) Anorthositic rocks of the Duluth complex: examples or rocks formed from plagioclase crystal mush. *J. Petrol.* **31**, 295–339.

Morse S. A. (1979a) Kiglapait Geochemistry I: systematics sampling and density. *J. Petrol.* **20**, 555–590.

Morse S. A. (1979b) Kiglapait Geochemistry II: petrography. *J. Petrol.* **20**, 591–624.

Morse S. A. (1982) Adcumulus growth of anorthosite at the base of the lunar crust. *Lunar Planet. Sci. XIII*. Lunar Planet. Inst., Houston. 10–18.

Morse S. A. (1986) Convection in aid of adcumulus growth. *J. Petrol.* **27**, 1183–1214.

Morse S. A. (1987) Origin of earliest planetary crust: role of compositional convection. *Earth Planet. Sci. Lett.* **81**, 118–126.

Morse S. A. (1988) Motion of crystals solute and heat in layered intrusions. *Can. Min.* **26**, 209–224.

Morse S. A. (1990) The differentiation of the Skaergaard intrusion: a discussion of hunter and sparks (Contrib. Mineral. Petrol. 95, 451–461). *Contrib. Mineral. Petrol.* **104**, 240–244.

Morse S. A., Brandy J. B. and Sporleder B. A. (2004) Experimental petrology of the Kiglapait intrusion: cotectic trace for the lower zone at 5 kbar in graphite. *J. Petrol.* **45**, 2225–2259.

Namur O., Charlier B., Toplis M. J., Higgins M. D., Liégeois J. P. and Vander Auwera J. (2010) Crystallization sequence and magma chamber processes in the ferrobasaltic Sept Iles layered intrusion Canada. *J. Petrol.* **51**, 1203–1236.

Namur O., Charlier B., Toplis M. J., Higgins M. D., Hounsell V., Liégeois J. P. and Vander Auwera J. (2011) Continuous differentiation of tholeiitic basalt to A-type granite in the Sept Iles layered intrusion Canada. *J. Petrol.* **52**, 487–539.

Namur O., Charlier B., Toplis M. J. and Vander Auwera J. (in press) Prediction of plagioclase-melt equilibria in anhydrous silicate melts at 1-atm. *Contrib. Mineral. Petrol*. doi:10.1007/s00410-011-0662-z.

Neumann G. A., Zuber M. T., Smith D. E. and Lemoine F. G. (1996) The lunar crust: global structure and signature of major basins. *J. Geophys. Res.* **101**, 16841–16843.

Nielsen T. F. (2004) The shape and volume of the Skaergaard intrusion Greenland: implications for mass balance and bulk composition. *J. Petrol.* **45**, 507–530.

Niu Y. and Batiza R. (1991) In situ densities of MORB melts and residual mantle: implications for buoyancy forces beneath mid-ocean ridges. *J. Geol.* **99**, 767–775.

Ochs F. A. and Lange R. A. (1997) The partial molar volume thermal expansivity and compressibility of H_2O in $NaAlSi_3O_8$ liquid: new measurements and an internally consistent model. *Contrib. Mineral. Petrol.* **129**, 155–165.

Ochs F. A. and Lange R. A. (1999) The density of hydrous magmatic liquids. *Science* **283**, 1314–1317.

Ohtake M. et al. (2009) The global distribution of pure anorthosite on the Moon. *Nature* **461**, 236–240.

O'Neill H. S. (1991) The origin of the Moon and the early history of the Earth: a chemical model. Part 1: The Moon. *Geochim. Cosmochim. Acta* **55**, 1135–1157.

Osborn E. F. (1959) Role of oxygen pressure in the crystallization and differentiation of basaltic magma. *Am. J. Sci.* **257**, 609–647.

Palme H., Spettel B., Jochum K. P., Drelbus G., Weber H., Weckwerth G., Wanke H., Bischoff A. and Stoffler D. (1991) Lunar highland meteorites and the composition of the lunar crust. *Geochim. Cosmochim. Acta* **55**, 3105–3122.

Philpotts A. R. and Carroll M. (1996) Physical properties of melted tholeiitic basalt. *Geology* **24**, 1029–1032.

Philpotts A. R., Shi J. and Brustman C. (1998) Role of plagioclase crystal chains in the differentiation of partly crystallized basaltic magma. *Nature* **395**, 343–346.

Philpotts A. R. and Dickson L. D. (2000) The formation of plagioclase chains during convective transfer in basaltic magma. *Nature* **406**, 59–61.

Pieters C. M., Tompkins S., Head J. W. and Hess P. C. (1997) Mineralogy of the mafic anomaly in the South Pole-Aitken Basin: implications for excavation of the lunar mantle. *Geophys. Res. Lett.* **24**, 1903–1906.

Putirka K. D. (2005) Igneous thermometers and barometers based on plagioclase + liquid equilibria: tests of some existing models and new calibrations. *Am. Mineral.* **90**, 336–346.

Raedeke L. D., McCallum I. S. (1980) A comparison of fractionation trends in the lunar crust and the stillwater complex. In *Proceedings of the Conference on Lunar Highlands Crust*, vol. 12 (eds. J. J. Papike and R. B. Merrill). *Geochim. Cosmochim. Acta Suppl.* pp. 133–153.

Robinson M. S. and Lucey P. G. (1997) Recalibrated mariner 10 color mosaics: implications for Mercurian volcanism. *Science* **275**, 197–200.

Scoates J. S. (2000) The plagioclase-magma density paradox re-examined and the crystallization of Proterozoic anorthosites. *J. Petrol.* **41**, 627–649.

Shearer C. K. and Papike J. J. (1999) Magmatic evolution of the Moon. *Am. Mineral.* **84**, 1469–1494.

Shearer C. K. and Papike J. J. (2005) Early crustal building processes on the Moon: models for the petrogenesis of the magnesian suite. *Geochim. Cosmochim. Acta* **69**, 3445–3461.

Shearer C. K., et al. (2006) Thermal and magmatic evolution of the moon. In *New Views of the Moon*, vol. 60 (eds. B. L. Jolliff, M. A. Wieczorek, C. K. Shearer, C. R. Neal), *Rev. Mineral. Geochem.* pp. 365–518.

Solomatov V. S. (2000) Fluid dynamics of a terrestrial magma ocean. In *Origin of the Earth and the Moon* (eds. R. Canup and K. Righter). Arizona Press, pp. 323–338.

Snyder G. A., Taylor L. A. and Neal C. R. (1992) A chemical model for generating the sources of mare basalts: combined equilibrium and fractional crystallization of the lunar magmasphere. *Geochim. Cosmochim. Acta* **56**, 3809–3823.

Snyder D., Carmichael I. S. and Wiebe R. A. (1993) Experimental study of liquid evolution in an Fe-rich layered mafic intrusion: constraints of Fe–Ti oxide precipitation of the T–fO_2 and T–ρ paths of tholeiitic magmas. *Contrib. Mineral. Petrol.* **113**, 73–86.

Sparks R. S., Meyer P. and Sigurdsson H. (1980) Density variation amongst mid-ocean ridge basalts: implications for magma mixing and the scarcity of primitive lavas. *Earth Planet. Sci. Lett.* **46**, 419–430.

Sparks R. S. and Huppert H. E. (1984) Density changes during the fractional crystallization of basaltic magmas: fluid dynamic implications. *Contrib. Mineral. Petrol.* **85**, 300–309.

Sprague A. L., Kozlowski R. W., Witteborn F. C., Cruikshank D. P. and Wooden D. H. (1994) Mercury: evidence for anorthosite and basalt from mid-infrared (7.3–13.5 μm) spectroscopy. *Icarus* **109**, 156–167.

Spudis P. D., Hawke B. R., Lucey P. G., Taylor G. J., Stockstill K. R. (1996) Composition of the ejecta deposits of selected lunar basins from Clementine elemental maps. *Lunar Plant. Sci. XXVI.* Lunar Planet. Inst., Houtson. #1255 (abstr.).

Sun S. S. and McDonough W. F. (1989) Chemical and isotopic systematics of oceanic basalts: Implication for mantle composition and process. In *Magmatism in the ocean basins*, Special publication 42 (eds. A. D. Sauders and M. J. Norry). Geological Society, London, pp. 313–345.

Tait S. R., Huppert H. E. and Sparks R. S. (1984) The role of compositional convection in the formation of adcumulate rocks. *Lithos* **17**, 139–146.

Taylor S. R. (1982) *Planetary Science: A Lunar Perspective*. Lunar Planet. Inst., Houston, p. 481.

Thy P., Lesher C. E., Nielsen T. F. and Brooks C. K. (2006) Experimental constraints on the Skaergaard liquid line of descent. *Lithos* **92**, 154–180.

Thy P., Lesher C. E. and Tegner C. (2009) The Skaergaard liquid line of descent revisited. *Contrib. Mineral. Petrol.* **157**, 735–747.

Toksoz M. N., Dainty A. M., Solomon S. C. and Anderson K. R. (1974) Structure of the Moon. *Rev. Geophys.* **12**, 539–567.

Tompkins S. and Pieters C. M. (1999) Mineralogy of the lunar crust: results from Clementine. *Meteorit. Planet. Sci.* **34**, 25–41.

Toplis M. J., Dingwell D. B. and Libourel G. (1994) The effect of phosphorous on the iron redox ratio viscosity and density of an evolved ferro-basalt. *Contrib. Mineral. Petrol.* **117**, 293–304.

Toplis M. J. and Carroll M. R. (1995) An experimental study of the influence of oxygen fugacity on Fe–Ti oxide stability phase relations and mineral-melt equilibria in ferro-basaltic systems. *J. Petrol.* **36**, 1137–1170.

Toplis M. J. and Carroll M. R. (1996) Differentiation of ferro-basaltic magmas under conditions open and closed to oxygen: implications for the Skaergaard intrusion and other natural systems. *J. Petrol.* **37**, 837–858.

Turner J. S. and Campbell I. H. (1986) Convection and mixing in magma chambers. *Earth Sci. Rev.* **23**, 255–352.

Vander Auwera J. and Longhi J. (1994) Experimental study of a jotunite (hypersthene monzodiorite): constraints on the parent magma composition and crystallization conditions (P, T, fO_2) of the Bjerkreim–Sokndal layered intrusion (Norway). *Contrib. Mineral. Petrol.* **118**, 60–78.

Verhoven J. and Schmalzl J. (2009) A numerical model for investigating crystal settling in convecting magma chambers. *Geochem. Geophys. Geosyst.* **10**, Q12007.

Warren P. H. (1985) The lunar magma ocean concept and lunar evolution. *Ann. Rev. Earth Planet. Sci.* **13**, 201–240.

Warren P. H. (1986) Anorthosite assimilation and the origin of the Mg/Fe-related bimodality of pristine moon rocks: Support from the magmasphere hypothesis. *Lunar Planet. Sci. XVI.* Lunar Planet. Inst., Houston. 331–343.

Warren P. H. (1990) Lunar anorthosites and the magma-ocean plagioclase-flotation hypothesis; importance of FeO enrichment in the parent magma. *Am. Mineral.* **75**, 46–58.

Warren P. H. (1993) A concise compilation of petrologic information on possibly pristine nonmare Moon rocks. *Am. Mineral.* **78**, 360–376.

Warren P. H. (2005) "New" lunar meteorites: implications for composition of the global lunar surface, lunar crust, and the bulk Moon. *Meteorit. Planet. Sci.* **40**, 477–506.

Warren P. H., Ulff-Moller F. and Kallemeyn G. W. (2005) "New" lunar meteorites: impact melt and regolith breccias and large-scale heterogeneities of the upper lunar crust. *Meteorit. Planet. Sci.* **40**, 989–1014.

Weinstein S. A., Yuen D. A. and Olson P. L. (1988) Evolution of crystal-settling in magma-chamber convection. *Earth Planet. Sci. Lett.* **87**, 237–248.

Wieczorek M. A. (2009) The interior structure of the Moon: what does geophysics have to say? *Elements* **5**, 35–40.

Wieczorek M. A. and Phillips R. J. (1997) The structure and compensation of the lunar highland crust. *J. Geophys. Res.* **102**, 10933–10943.

Wieczorek M. A. and Phillips R. J. (1998) Potential anomalies on a sphere: applications to the thickness of the lunar crust. *J. Geophys. Res.* **103**, 1715–1724.

Wieczorek M. A. and Zuber M. T. (2001) The composition and origin of the lunar crust: constraints from central peaks and crustal thickness modeling. *Geophys. Res. Lett.* **28**, 4023–4026.

Wieczorek M. A., et al. (2006) The constitution and structure of the lunar interior. In *New views of the Moon*, vol. 60 (eds. B. L. Jolliff, M. A. Wieczorek, C. K. Shearer and C. R. Neal) *Rev. Mineral. Geochem.* pp. 221–364.

Wood J. A. (1986) Moon over Mauna Lea: a review of hypotheses of formation of Earth's Moon. In *Origins of the Moon* (eds. W. K. Hartman, R. J. Philipps and G. J. Taylor). Lunar Planet. Inst., Houston, pp. 17–55.

Wood J. A., Dickey J. S., Marvin U. B., Powell B. N. (1970) Lunar anorthosites and a geophysical model of the Moon. *Lunar Planet. Sci. I.* Lunar Planet. Inst., Houston. 965–988.

Associate editor: Randy L. Korotev